2018-01-01

A Novel Method For Fabricating Material Extrusion 3D Printed Polycarbonate Parts Reinforced With Continuous Carbon Fiber And Improvement Of Strength By Oven And Microwave Heat Treatment

Md Naim Jahangir
University of Texas at El Paso, naim.buet09@gmail.com

A NOVEL METHOD FOR FABRICATING MATERIAL EXTRUSION 3D PRINTED POLYCARBONATE PARTS REINFORCED WITH CONTINUOUS CARBON FIBER AND IMPROVEMENT OF STRENGTH BY OVEN AND MICROWAVE HEAT TREATMENT

MD NAIM JAHANGIR

Master's Program in Mechanical Engineering

APPROVED:

David Espalin, Ph.D., Chair

Ryan Wicker, Ph.D., Co-Chair

Juan Noveron, Ph.D.

Charles Ambler, Ph.D.
Dean of the Graduate School

Dedication

This Thesis is Dedicated to My Beloved Father Mohammad Ali Mondal (1951-2011), Mother- Firoza Khatun, and My Elder Brother- Md Nashmush Shakib Who Literally Sacrificed Everything So That I Can Get a Better Educational Environment. I Want to Thank Maisha Mumtahana and Neli Sultana for Being Always Very Affectionate to Me.

A NOVEL METHOD FOR FABRICATING MATERIAL EXTRUSION 3D PRINTED POLYCARBONATE PARTS REINFORCED WITH CONTINUOUS CARBON FIBER AND IMPROVEMENT OF STRENGTH BY OVEN AND MICROWAVE HEAT TREATMENT

By

MD NAIM JAHANGIR, B.Sc. in M.E.

THESIS

Presented to the Faculty of the Graduate School of

The University of Texas at El Paso

in Partial Fulfillment

of the Requirements

for the Degree of

MASTER OF SCIENCE

Department of Mechanical Engineering

THE UNIVERSITY OF TEXAS AT EL PASO

August 2018

Acknowledgements

I want to acknowledge the effort, and guidance of my supervisor Dr. David Espalin, assistant professor, department of mechanical engineering, University of Texas at El Paso (UTEP). I am also grateful to Dr. Ryan Wicker, director of the W.M. Keck Center for 3D Innovation, for letting me work in one of biggest lab for 3D printing with craziest research facilities. Special thanks go to Dr. Yirong Lin and Dr. David A. Roberson for their influence in my research. I want to thank Dr. Ahsan Choudhuri and Syeda Nargis, for always helping me out with my problems. I am grateful to my lab mates: Carlos Acosta, Steven Ambriz, Kazi Md Masum Billah, Jose Coronel, Xavier Fernandez, Lluvia Herrera, Dr. Mohammed Shojib Hossain, Jose Motta, Mireya Perez, Leonardo Gutierrez Sierra for both helping and teaching me about 3D printing and characterizations. Special thanks goes to Syed Zia Uddin, Ashiqur Rahman, Asad Gulib, Suhail Mahmud, Mashriq Ahmed Saleh, Shaimum Shahriar, Swadipto Roy, Fazle Rabbi, Mirza Mohammad Maqbul Elahi, Tanvir Hossain Polok, and to everyone for whom I never felt that I was 8500 miles away from my home. Finally, I am grateful to my almighty for blessing me with such wonderful parents.

Abstract

The study of continuous carbon fiber-based material extrusion FDM printed materials can eliminate the problem of lower strength of additive manufactured part. Additive manufacturing, the process of fabricating complex shaped specimen with a layer-by-layer manufacturing technique, is being utilized in industrial application rapidly. Though the biomedical application may not be literally dependent on strength property, the factor is not deniable for the structural uses of 3D printed polymers. Insufficient neck growth and adhesion between layers are the driving factors of lower strength. The presence of porosity in the 3D printed parts is a major drawback and studies showed that the relation between porosity volume fraction and mechanical strengths (tensile, flexural, and compressive) is inverse. The concept of fiber reinforcement, which is common in conventional manufacturing system, has not been studied yet in 3D printing. A lot of work has been done on heat treatment (both pre and post) of fiber reinforced polymers for injection molded and other convention techniques. To authors' best knowledge no work has done on fabricating material extruded polycarbonate with embedded continuous carbon fiber. Moreover, no work has been done on heat treatment of FDM printed polymers.

In the current study, a novel technique is introduced to embed CF in 3D printed parts at different layers. Four different kinds of ASTM D638 Type I samples were prepared: PC with no CF (neat PC), PC with one bundle CF (at seventh layer), PC with two bundles CF (at fifth and ninth layers), PC with three bundles CF (at fourth, seventh, and tenth layers). Note that, total number of layers were 13 and the embedding operation was done manually with the minimum (one drop per carbon fiber) use of adhesives. Application of heat was through a Kapton film on PC-CF surface, resulted in improved bonding between PC, and CF. Fiber pull out tests show that bond strength (pull out force) between PC-CF was higher than the breaking strength of CF (400 to 475 N) showing that fiber broke before it could be pulled out from the composite. Embedding CF, without any cavity, resulted in maximum 13.9%-dimensional inaccuracy along thickness whereas the error was negligible along length and width. 3D printed polymers showed warp behavior due

to residual, and thermal stresses work on the specimen during printing and the thermal mismatch of PC (having positive thermal expansion rate) and CF (having negative thermal expansion rate). Regardless of number of embedded CF bundle, all specimens (with CF) showed similar warp properties. PC with three bundles of CF (0.04 by volume fraction) (47.9 MPa) showed 77% higher tensile yield strength than neat PC specimen (27.1 MPa). PC with three bundles of CF (3.36 GPa) showed 85% higher modulus than the neat PC specimens (1.82 GPa). One of the unique findings of the study is printing of specimens with eight layers (out of 13) where no void was visible under microscopic observation. The cavity less embedding of CF created disturbance in the printing process and the extra filament materials, under higher pressure due to height mismatch exerted from nozzle, filled the void portions.

Another important part of this thesis is the post processing heat treatment (HT) of FDM printed parts. Three different HT processes were applied: water boiled, oven, and microwave (MW) HT. To authors' best knowledge no previous work have been done on MW treatment of any 3D printed polymers and, again, no study can be found for all three HTs of 3D printed composites. HT didn't have significant impact on dimensional accuracies (for both dimensional and warp behaviors). But when tensile yield strength was studied, MW heat treated PC with one bundle (44.5 MPa), two bundles (55.9 MPa) and three bundles CF (60.2) showed 64%, 106%, and 122%, respectively, increase than the neat PC specimen with HT (27.1 MPa). The most important part was the strength of 3D printed MW treated PC with three bundles CF showed similar tensile yield strength of neat PC specimens fabricated using conventional techniques (63 MPa). MW and oven heat treated PC with three CF bundle specimens (3 and 2.5 GPa, respectively) showed 65% and 37% increase in modulus of elasticity than the neat PC but the improvement was identical to the untreated PC with same configuration. Flexural strength and modulus of MW treated PC with three bundle CF (58.8 MPa and 1.5 GPa, respectively) were 20.5% and 18% higher than untreated neat PC parts (48.8 MPa and 1.27 GPa, respectively). MW treated PC with three CF bundles showed brittle fracture behavior and microstructure of cross section showed significant regions without porosity.

Table of Contents

List of Tables

List of Figures

Chapter 1: Introduction

1.1 Background

1.1.1 3D printed polymer composites

The ability of fabricating functional parts containing complex geometrical shapes in a reasonable period and reduced product development cycle time, influence the faster growth of additive manufacturing technology. The increasing demand of fabricating 3D printed fixtures and functional parts with and without embedded sensors and circuits are driving the need of geometric accuracy with less build time, cost management and higher strength of additive manufactured parts. Where in literature, a lot of work has been done on improvement of mechanical strength of conventional polymers by fiber reinforcement, very few works have been done on reinforcement of material extrusion polymer parts. The conventional carbon fiber (CF) reinforced polymer showed improved mechanical (both tensile and flexural) strengths and the advantages of high strength-to-weight ratio drives its applications in sensor, automotive, aerospace, and structural sectors. For example, Boeing is using CF (TORAYCA Prepreg P2302) reinforced plastics to fabricate empennage and floor beams of B777 [1]. Recently, Stratasys, a 3D printing production-oriented company, is fabricating automotive parts e.g.: car dashboard, mounting casing for braking components with cooling application using CF reinforced 3D printed nylon composites. A lot of application of material extrusion polymers are seen that emerges the need to reinforce the fabricated part. Road Shop, another industry for production, is using 3D printing technology to fabricate custom gauge cluster for Datsun 620 model car. Industries like Brooks and Ecco has already produced footwear with innovative design using 3D printing technology. Different polymers have been used for material extrusion technology and among them Polycarbonate (PC)

has a higher glass transition temperature of 147°C when compared to most of the available polymers for material extrusion, used in 3D printing, e.g: ABS [105°C], PS [100°C], nylon-6 (47°C), PLA (65°C). The tensile yield strength and flexural strength of conventional injection molded PC parts are 63 and 89.6 MPa, respectively. In 3D printing, a layer-by-layer manufacturing process, specimen strength is much lower due to weaker adhesion between layers and presence of porosity. Continuous CF embedded 3D printed polymer composites can increase strength of 3D printed materials as Voigt model states based on Hooke's law and equal strain assumption. The rule composed of terms V, E, σ, and ε representing volume fraction, modulus, stress, and strain, respectively and states that-

$$\text{effective strength}, \sigma = \sigma_{PC} V_{PC} + \sigma_{CF} V_{CF}$$

$$\sigma = E\varepsilon$$

The model doesn't acknowledge the presence of porosity in the fabricated part. Porosity, a major drawback occurs due to insufficient neck growth of filament beads, adversely affects the strength property of 3D printed parts. A study of compressive strength of 3D printed alumina-ceramic scaffolds reported ~96% increase in compressive strength with pore volume fraction was reduced from 0.44 to 0.29% [2]. The application of CF without any cavity can be handful to remove porosity by proper placement of excess material that can be placed if CF was not embedded, into the pores. The current study developed a method to embed continuous CF manually to increase material strength and reduce porosity by the addition of CF as a disturbance.

1.1.2 Importance of embedded CF in 3D printed parts

The study of fiber reinforced polymers has been given much importance over past half centuries. The advantage fabricating parts with high strength-to-weight and low strength-to-cost ratios, are the reasons of wide use of fiber reinforced polymers in automotive, aerospace and

structural applications. In conventional fabrication processes e.g. injection molding, melt blending, hot pressing of fiber reinforced polymers, carbon nano tubes (CNTs), short carbon fiber (SCF), continuous carbon fiber (CCF), natural fiber (bamboo), glass and Kevlar fibers are widely used [3]. Natural fibers received much attraction because of lightweight, nonabrasive, combustible, non-toxic, low cost, and biodegradable properties. Lack of good interfacial bond, low melting point, and poor resistance to moisture made it less user friendly. Upon chemical treatments, strength property of natural fibers decreased because of the breakage of the bond structure and the disintegration of the non-cellulosic materials [3]. CF based composites showed improved mechanical properties than other fiber-polymer composites. Fu et al. (2000) [4] reported that the tensile yield strength of glass fiber and CF fiber reinforced polypropylene are 18 and 44 MPa, respectively. Another reason to use CF over glass fibers is glass fiber-based composite shows more brittle behavior upon fracture. Carbon fiber /epoxy (Hexcel T300/914) reinforced polymer is the most used fiber based composite type for aerospace application with an allowable compressive strain of <0.4% [5]. CF reinforced styrene is used as a shape memory polymer composite (SMPC) and SMPC is also used as a deployable structure. Fiber reinforced shape memory polymer has the advantages of high strain recovery and higher strength (thanks to the application of CF) [6]. Short CF (SCF) based polymer composites are used in making automotive industries. Conventional 10% SCF reinforced Polypropylene composites, processed using melt blending and hot-pressing techniques, was used to fabricate car bonnet and strength were comparable with carbon steel [7]. As 3D printing can manufacture smooth and innovative parts with complex design, the application of CF based material extruded composites are sure to control the future generation production process.

1.1.3 Importance of post processing heat treatment of 3D printed parts

Heat treatment (HT) of polymer composites near glass transition temperature softens the polymer matrix helping better bonding with CF. Conventional oven HT requires three times more HT period than Microwave (MW) HT for attributing same polymer softening effect. The higher absorption coefficient of CF has major impact of HT application which helps to improve bonding between CF and polymer. Microwave can penetrate material as the energy is transferred by the interaction of molecules with the electromagnetic field. The energy transfer is highly depended on the higher dielectric loss and absorption properties of specimen. Different pre and post processing heat treatment (HT) processes have been applied to improve the strength of conventional polymer composites. So far, the interaction of HT to CF has been fruitful as the heat is absorbed by the CF and creates enlarged, and rougher fiber planes. Experiments showed that enlarged and rougher fibers have better adhesion with the matrix material due to the impact of friction. One important aspect of MW treatment of CF as it increases wettability of CF. That works as a chemical treatment and ensures improved bonding [8]. Pre-processing HT is the process of curing CF at a specific temperature with or without flow of Argon, Nitrogen, oxygen etc gases. Post processing HT of fabricated parts with oven or microwave (MW) treatment.

Other than post processing curing of stereolithography and selecting laser sintering (SLS) parts, no work has been done on the HT of 3D printed parts. Post processing MW HT of FDM printed CF/PC polymer composite should serve the purpose of both pre and post process HT. The presence of porosity in the parts should allow MW to interact with CF directly and improve its property. Note that, MW can penetrate surfaces even in parts with zero void. The presence of pore should also be effective for oven HT because the transfer of heat energy can reach the inside part and modify CF with rougher and enlarged surface which is helpful for improved bonding.

1.2 Literature review

1.2.1 CF reinforced conventional composites

Even though the thesis is on the reinforcement of 3D printed polycarbonate with CF, the study of conventional composites is important to compare the process parameters and strength behavior. The application of fibers, from CF to modified pretreated CF to carbon nano tube (CNT) has shown a rise of improved tensile and flexural strengths. Carneiro et al. (1998) [9] used a flow reactor immerged with methane to fabricate vapor grown carbon fibers (VGCF). The CF was compounded with PC in a twin-screw extruder and the composite was produced by injection molding. Five different sets of composites were produced with 5, 10, 20, and 30 wt% (w/w) VGCF. PC with 20% VGCF composite exhibited 39% improvement of modulus and 17% increase of yield stress. Note that, PC with 30% VGCF showed brittle behavior and it fabricated imperfect parts with rough surfaces because of excessive CF did not bond perfectly with the polymer. Fu et al. (2000) [4] pre-treated fibers by feeding short glass fiber (SGF) and short carbon fiber (SCF) separately into melted polypropylene (PP) using a twin extruder and the compounded extrudates, were immediately quenched and cooled before being chopped. Finally, tensile bars were prepared using injection molding technique. A modified equation for the rule of mixture was introduced by using two new factors for both modulus and strength. SCF/PP and SGF/PP composites, both with 25% fiber volume fraction, exhibited ultimate tensile strength of 60 MPa and 49 MPa, respectively. Note that, for both the composites brittle fracture nature was observed from both fracture surface and stress- strain diagram. Kuriger et al. (2001) [10] processed vapor grown CF to reinforce polypropylene and found fiber orientation is important for bonding but has little impact on modulus. Fiber-polymer mixture was blended using a Leistritz LSM 30.34 twin-screw laboratory extruder to disperse CF in polymer. VGCF/PP composite was extruded at approximately 280-

290ºC and screw speed was 80 rpm. Result showed that at fiber volume fraction 0.11, ultimate tensile strength (UTS) of the specimens prepared with 5.25 cm nozzle and 1.25 cm nozzle were 68 MPa and 54 MPa, respectively. But once the fiber volume fraction was decreased to 0.025, UTS decreased to 46 MPa and 41 MPa, respectively, showing strength decreased with the reduction of both of nozzle diameter and CF volume fraction. Hasimoto et al. (2012) [11] studied both experimental and micromechanics of PP composite reinforced with discontinuous CF. A layer-wise method (LWM) was developed for predicting the UTS of composites with varying length of SCF and arbitrary angle orientation. The approach introduced two modifying factors, strength and modulus, during strength calculation of composites. Results showed that fiber length has significant impact on tensile strength. The ultimate tensile strength of 20% volume fraction SCF reinforced PP composites with fiber length 2 mm and 6 mm were 230 MPa and 295 MPa, respectively. So optimum choice of CF length, volume fraction, extruding temperature, and nozzle diameter of extruder resulted in higher tensile strength and modulus.

1.2.2 Continuous fiber reinforced 3D printed polymer composites

Though a lot of work have been done on reinforcement of conventional extruding and injection molding, a little can be found on 3D printed composites reinforced by continuous fiber. Importance have been given on CF as a reinforcement while only a few can be found with Kevlar fiber. CF reinforced 3D printed thermoplastics can provide higher strength-to-weight, and stiffness-to-weight ratios with the advantages fabricating complex parts with innovation in design.

Tian et al. (2016) [12] proposed a novel technique for fabricating continuous carbon fiber (CCF) reinforced thermoplastic (PLA) composite. Polylactic (PLA/ 1.75 mm) and CF (1000 fibers in a bundle) were deposited simultaneously to print part with dimension 100 mm × 15 mm × 2 mm. Optimum printing parameters for better quality printing were proposed by varying factors

like liquefier temperature, layer thickness, feed rate of filament, hatch spacing, transverse movement. Liquefier temperature was below 180ºC showed difficulties in printing. But when it was ~240°C, PLA filament flowed smoothly. Layer thickness was varied from 0.3 to 0.6 mm and maximum flexural strength was found 240 MPa at 0.3 mm thickness. When the hatch spacing varied from 1.8 to 0.4 mm, flexural strength increased from 130 to 335 MPa. Fiber content was varied and when the content reach 27% with optimum hatch spacing and temperature properties, flexural strength and modulus increased to 335 MPa and 30 GPa, respectively. Finally, a single wall cylindrical shaped CF/PLA part was fabricated in one process cycle with continuous embedding of CF bundle highlighting the fact that this technique can be potentially utilized in aviation and aerospace sections.

Li et al. (2016) [13] manufactured CF reinforced PLA composites with rapid prototyping approach with novel extrusion nozzle and path control methods using a desktop FDM. The work suggested that the weak interface bonding between CF bundle (1000 fibers in one bundle) and PLA lowers the strength and there arises the need improved bonding between polymer and CF. Samples were fabricated with both modified, and unmodified CF. The strength and thermodynamics properties were evaluated by the electronic testing machine and dynamic mechanical analyzer (DMA). The surface modification of CF bundle was conducted before the printing started by keeping it in a emulsified, and processed solution of methylene dichloride and 8% mass fraction PLA particles. Finally, 13.8% and 164% improvement of tensile (specimen dimension 110 mm × 27 mm × 2.3 mm) and flexural (specimen size 35 mm × 12 mm × 2.3 mm) strengths were observed, respectively, for modified CF reinforced composite compare to the strength of unmodified CF reinforced PLA composite.

Goh et al. (2017) [14] used fused filament fabrication material extrusion process to fabricate glass fiber and carbon fiber reinforced nylon composites. Printing parameters included printing temperature of 260°C, layer height of 0.1 mm and unidirectional pattern (0 degree). ASTM D790-15e2 standard was used for flexural test and fiber direction was changed by 45° from each layer to the next one (0°-45°-90°-45°) for 14 layers. Specimen with 45% CF volume fraction showed the volume fraction of CF affects the strength which is identical to conventional composites. The flexural strength of the composite was 420 MPa which was 292% higher than the maximum strength of conventional neat nylon (107 MPa). ASTM D3039M-14 standard was used for tensile test and result showed the specimen failed at 530 MPa at 5.2% strain which is ~560% higher than the UTS of neat nylon specimen (80 MPa). From microstructure, fiber breakage was observed with tensile rapture and matrix crack due to shear rapture that initiated fracture of specimen. Another notable thing was fiber breakage initiated at outer most CF layer and then it propagated to initial layers.

Yang et al. (2017) [15] fabricated CCF reinforced ABS parts using an FDM desktop printer. The printer has the advantage of simultaneous deposition of both CF and extrusion material. Printing parameters were maintained at 0.5 mm of layer thickness, extrusion temperature of 230°C, envelope temperature 90°C, for optimal quality. Three different tests: three-point bending test, flexural test and tensile tests were done to characterize material properties of continuous CF/ABS composites. The filament diameter of ABS was 1.75 mm and 1000 fibers per bundle was used for CF. Four different samples were prepared: FDM printed ABS with and without continuous CF, and injection molding ABS with and without CF. Flexural strength of neat ABS and 3D printed CCF/ABS composite were 65 MPa and 127 MPa, respectively. The strength of 3D printed CCF/ABS was 40% lower than injection molded CCF/ABS (177 MPa) composite.

The UTS of 3D printed neat ABS, and CCF/ABS composites were 27 and 150 MPa, respectively. The UTS of 3D printed composite was 33% lower than injection molded CCF/ABS composite part (200 MPa).

Melenka et al. (2016) [16] used a commercially available desktop material extrusion 'Markone' by Mark Forged with the advantages of both printing and embedding fibers to fabricate Kevlar reinforced nylon composite. ASTM D638-14 Type I specimen was printed and Kevlar fiber rings were embedded on certain pauses. Samples with zero, two, three, four and five Kevlar rings were printed, and the volume fractions of the fibers were 0, 4.04, 8.08, and 10.1%, respectively. Note that, printing was completed in total 32 layers. Results showed UTS increased gradually with increased number of rings and for zero, two, four, and five the UTS were 25, 32, 58, and 80 MPa resulting in maximum 220% increase in UTS when compare to neat 3D printed nylon part. Identical improvement trend was maintained for elastic modulus and the value for nylon with two, four, and five fiber rings were 1767.2, 6960.0, and 9001.2 MPa, respectively. The first two moduli were less than the predicted modulus. Specimen failed near notches and micrograph showed that failure occurred at the starting edge of fiber reinforcement. Lack of wetness of fiber rings and insufficient bonding between nylon surface and fiber rings with misalignment caused reduction of strength. So the study of material extruded CCF/polymer composite shows improvement in mechanical strength.

1.2.3 Short fiber reinforced 3D printed polymer composites

While the principal of embedding continuous fiber in 3D printed composite is to add a pause in the printing process and to place fiber, the short fiber application process is totally different. From literature, only short carbon fiber (SCF) was used to reinforce 3D printed

composites and like CCF, small amount of work have been done on 3D printed SCF/thermoplastic composites.

Ning et al. (2015) [17] processed carbon fiber reinforced polymer feedstock filaments to fabricate 3D printed parts. The entire process of fabricating short fiber reinforced polymer had two parts; firstly, preparing filament with the combination of pellets and small fibers and finally, using the filament in FDM material extrusion to print specimen. In the referred work, ABS thermoplastic pellets and CF were mixed and blended together. Note that, CF powders of two distinct sizes were used: 150 μm and 100 μm and different wt.% of SCF (3, 5, 7.5, 10, 15 wt.%) was blended with the ABS pellet. An extruder (EB-1, ExtrusionBot Co. Chandler, AZ, USA) was used to prepare the filament. The process parameter included 220°C extrusion temperature, 2 m/min filament yield speed and 2.85 mm nozzle diameter. An FDM 3D printer was used to print ASTM D638-10 tensile and ASTM D790-10 flexural specimens. The results didn't agree that increase of CF volume would necessarily improve tensile properties. The UTS of neat ABS specimen and 15 wt.% specimens were 33 and 37 MPa and maximum UTS (43 MPa) was obtained for 5 wt.% SCF reinforced ABS specimen. Maximum young's modulus was found for 7.5 wt.% SCF/ABS specimens (2.5 GPa) and it was 32% more than the neat ABS (1.9 GPa). Specimen with 5 wt.% SCF, showed 11.82, 16.82, and 21.86% improvement of flexural stress, flexural modulus, and flexural toughness, respectively. Microstructure showed that with increased SCF content, individual pore size also increased and resulted in lower strength. Another problem was observed as many SCF seemed to pull out of the matrix with the increase of SCF content and the fact explains the lower strength of specimens with 10 and 15 wt.% SCF. The same principal was utilized by Tekinalp et al. (2014) [18] to reinforce 3D printed ABS with short CF. Chopped Hexcel AS4 CF was used of 3.2 mm (long) and GP35-ABS-NT ABS copolymer were used to prepare filament for extrusion. A

Brabender Intelli-Torque Plasti-Corder prep-mixer was used to blend ABS and CF at 220°C with a rotor speed of 60 rpm. Mixtures were prepared with 0, 10, 20, 30, and 40 wt.% SCF with an average mixing time of 13 min. A plunger type batch extrusion was used to prepare filament of 1.75 mm diameter. ASTM D638 Type V parts were printed with all five different filaments with different volume fraction. Note that, due to clogging problem of FDM print head, it was not possible to print SCF/ABS composite with 40 wt.% SCF. Printing parameter included 205°C nozzle temperature, 85°C table temperature, 0.2 mm layer height. Micrograph showed that neat ABS specimen showed consistent voids but specimen with 10 wt.% SCF, showed less amount of porosity. Noticeable thing was protruding SCFs were clear of matrix material and indicated poor interfacial adhesion between CF and ABS. Pore size was seen around the fibers but larger pore size with increase of layers was not visible. Tensile result showed SCF (30 wt.%)/ABS specimen showed 25% and 76% improvement of strength than 10 wt.% SCF/ABS composite and neat ABS specimen, respectively.

The study of 3D printed composites reached to carbon nanotube (CNT) as reinforcement. Shofner et al. (2003) [19] used both single wall carbon nanotubes (SWNTs) and vapor grown carbon fiber (VGCFs) with ABS to print composites using Extrusion Freeform Fabrication (EFF). SWNTs (Tubes@Rice, Houston, TX) were produced using pulsed laser vaporization technique. VGCFs were treated to remove dust and impurities and for surface functionalization, surface was prepared using hydroxyl, carboxyl, hydrocarbons, and quinone groups. Micrograph showed that VGCFs aligned perfectly in the direction of extrusion. When the reinforcement content was 5 wt%, VGCFs/ABS and SWNTs/ABS composites showed ~44% and ~93% increase in modulus of elasticity, respectively. The tensile property showed ~24% and ~50% improvement of tensile strength (for 5 wt% volume fraction of reinforcement) of VGCF/ABS and SWNT/ABS,

respectively, than the unfilled ABS sheet. So, the optimum use of SCF and SWNT showed higher tensile strength of 3D printed composites.

1.2.4 Drawbacks of 3D printed parts

1.2.4.1 Strength

In layer-by-layer operation, insufficient bond between filaments negatively influence the mechanical strength of 3D printed specimen. Again, the weak interlayer strength becomes weaker in the building direction. Thermal energy of the extruded material drives the bonding quality and strength property. The neck growth between the adjacent filaments highly relies on molecular diffusion and increased neck growth is key to stronger specimen [20]. Sood et al. (2010) [21] pointed out several factors that affects the material strength. With increased porosity and volumetric shrinkage, decreased load bearing area cause immature failure of specimen. The work varied number of layers and found tensile strength increases with increased number of layers. When layer numbers were less, minimization of distortion at bottom layers were significant. With the increase of layers, distortion effect was minimized since distortion due to temperature was subjected with the presence of lower number of layers.

Almost all the printing parameters has impact on strength but few of them controls the strength property. Ahn et al. (2002) [22] showed that process parameters such as air gap and raster orientation affect the tensile property of FDM parts significantly. Parameters like raster width, model temperature and color have negligible impact on strength property. FDM P400 was used and with -0.08 mm (-0.003 inch) overlap between roads improved tensile strength to ~72% of the value of injection molded ABS P400. Compressive strength of the 3D printed materials with same road width was ranged between 80 to 90% of the injection molded ABS. Axial specimens with 0

raster angle (19 MPa) showed 52% improvement of tensile strength that specimen printed at 45/-45 raster angle (12.5 MPa). Compressive strength of axially build specimen (38 MPa) was 19% higher than the one build in the transverse direction (32 MPa). Lee et al. (2005) [23] found that factors like layer thickness, raster angle, air gap have impact on the elastic performance of 3D printed FDM parts. Nine different prototypes were printed using ABS material and results were analyzed by employing two main effect: ANOVA and signal-to-noise ratio. Motivation was to achieve maximum elastic performance and that was achieved at angle of displacement of 15. Gurrala et al. (2014) [24] observed the relationship strength and volumetric shrinkage of ABS printed specimen. Pareto optimal model showed that when volume shrinkage was 0.85%, strength of the ABS specimen was 24 MPa but when it 5.8%, strength increased to 36 MPa resulting in a 50% improvement of the strength. So, optimizing major printing factors of each FDM is a prerequisite for maximum strength.

1.2.4.2 Porosity

The presence of porosity in additive manufactured part was always been a concern. In polymer material extrusion, the insufficient neck growth, due the unavailability of heat and time, attribute to porosity. Sun et al (2005) [25] described the temperature profile of 15 and 30 layered ABS specimens and experiments showed that temperature of the filament of the first layer few layers rises above the glass transition temperature (210°C). Each pick position of temperature experienced a rapid decrease when extrusion head goes far from the printing specimen. By the time nine layers were completed, temperature ranged between 100 to 115°C and the rest of the part was printed within that temperature range. So, the neck growth of the bottom layers was more than the few in the top layers resulting in increasing pore size in the building direction.

Though in biomedical engineering and tissue scaffold study, controlled pore size is desirable because of the surface roughness created by pore is helpful for nutrient movement and bone tissue growth [26], however the porosity is highly undesirable in structural and industrial applications. Kalita et al. (2003) [27] focused on the development and fabrication of controlled porous parts. The parts were particulate reinforced and developed by mixing polypropylene (PP) and tricalcium phosphate (TCP) ceramics. Pore size was controlled by a commercially available FDM by controlling the road width, slice thickness and road gap (0.76, 1.02, and 1.27 mm). Three different samples were prepared, with 36, 40, and 52 vol.% porosity, with an average pore size of 160 μm. When pore size (radius) was varied having constant overall porosity volume, compression strength was unchanged. But when the overall volume % of porosity was varied, keeping the pore size constant, strength property changed rapidly. Specimens with 36, 40, and 52 vol.% porosity showed the compressive strength of 12.7, 9, and 8.7 MPa, respectively. A 12% increase in modulus was also seen of when porosity vol.% was reduced from 52 to 36%. Chin Ang et al. (2006) [28] investigated the relationship between compressive strength and porosity of FDM printed ABS scaffold. Printing parameters included: air gap 0 to 1.27mm, raster width 0.305 to 0.98 mm, build orientation 0 to 90°. Results showed that at 80% porosity, yield strength was 4 MPa and at 30% porosity, yield strength was 30 MPa resulting in 650% improvement of strength due to significant reduction of porosity. Thus, the further study of porous less 3D printed specimen can bless the technology with improved strength.

1.2.5 Dimensional mismatches of 3D printed polymers

1.2.5.1 Dimensional inaccuracy

One of the major drawbacks of FDM printed parts is its inability to print parts with 100 %-dimensional accuracy. The problem is understandable because of the neck growth of filament beads in each layer is subjected to varying temperate resulting in variable thermal expansion. Pennington et al. (2003) [29] analyzed the dimensional accuracy of FDM2000 printed ABS parts. An analysis with 12 different samples concluded that the effect of part size, location of printing in the build platform, and envelope temperature have significant effect on inaccuracy. The work was done by printing parts with six features: overhang, horizontal boss, horizontal cylinder, vertical boss, vertical cylinder, and thin wall. But location of part in the chamber and envelope temperature caused maximum percentage of inaccuracy. On the other hand, part orientation, road width, and layer thickness have less effect on inaccuracy. It was stated that cooling rate and air flow inside the FDM chamber are also responsible for the inaccuracy, but no data was presented on it.

Dao et al. (1999) [30] used a shrinkage compensation factor to print specimen with desired dimension. As ABS P400 has a specific thermal contraction rate, the part was printed with the modified dimension by multiplying the CAD dimension with shrinkage compensation factor (SCF). A SCF factor of 1.007 resulted in reduction of 53% error. Note that, the accuracy of Stratasys FDM 1650 is ±0.127 mm and SCF should vary depending on the accuracy of every different FDM. The work concluded that better result is possible if separate SCF can be defined along x and y axis. Volpato et al. (2014) [31] studied the influence of surface profile on dimensional accuracy in the Z-axis in FDM printed parts. An FDM 2000 was used to manufacture a rectangular part with dimension 10 mm × 15 mm × 2 mm using ABS P400 as modelling and ABS P400R as support material. Same parts were printed using five layers for support and default

support of four layers but didn't result in smoother surface. Another approach was utilized with three of first five support layers were printed first, and the fourth layer was deposited transversally to the third and the fifth transversally to the fourth. The second approach printed visually best quality parts. Results showed that improvement of surface quality of the support material increases the accuracy percentage of printed parts up to 50% along Z-axis. This is still a wide-open sector of material extrusion for further research.

1.2.5.2 Warpage

FDM printed polymer components shows significant amount of warp behavior. The term warpage refers to bending of specimen due to the change of thermal gradient while printing. Further study is needed to characterize warp phenomena. Both analytical and simulation models have failed to quantify the effect of different parameters on warpage. Factors like in-plane, and vertical dimensions, layer thickness showed different warp properties depending on the part geometry. In modelling, the study is difficult for complex geometries due to the unavailability of proper equations and boundary conditions which recognizes the unavailability of mathematical formulas that recognizes porosity factor of FDM parts. The 2D model for quantifying warpage assumes each point of the part is subjected to constant horizontal plane stress and the last layer is at constant temperature [32].

Armillotta et al. (2018) [33] described the warpage phenomena by the printing temperature during material extrusion process and cooling down of the parts to the surrounding temperature after fabrication. The cooling process of polymer causes shrinkage, but the build platform tries to prevent that contraction. That develops a stress gradient with both tensile and compressive portions. When the part is removed from the build platform, stress released and bending distortion is created on the opposite direction of that stress gradient. FDM printed ABS

rectangular plate was prepared and it showed that thermal distortion is significant along the edge of the part. Another technique was applied by increasing layer thickness for same specimen and the latter showed less warpage (wasn't quantified) because the increase in thickness made the part more resistant to bending. Gregorian et al. (2001) [34] suggested build speed and printing temperature induces residual stresses in the both building platform and printed materials and concluded that these two factors are responsible for inducing more warpage to the specimen.

1.2.6 Micro wave heat treatment of CF reinforced conventional composites

Microwave treatment of fiber reinforced composites have been utilized since 1960s for improved mechanical strength of composites. A bunch of work has been done on that era to improve fiber properties for both textile and composite applications. Li et at. (1997) [35] observed that the main purpose of MW treatment of fibers is to improve the physical, and chemical properties of fiber and to improve bonding between fiber and matrix, without influencing bulk properties. The physical property is modified by engaging roughness to the fiber which produces larger fiber contact area. The effect is known as sputtering effect. The chemical modification works by the implementation of polar groups and their activeness on the fiber surface. The effect reduces surface energy and promotes improved bonding the fiber and polymer. Generally, adhesion between fiber and matrix is evaluated by micro-bond or mon-filament pull-out test. Biro et al. (1993) [36] reported that after air MW plasma treatment, interfacial shear strength was increased by 118%. The strength was determined by a micro-bond test. Note that polyethylene, 828 epoxy resin, and 45% Kevlar fiber were used for fabricating the composite.

Jang et al. (1992) explained the need of controlling adhesion during MW plasma treatment in continuous carbon and Kevlar fibers. In cold plasma treatment, excessive exposure of CF to oxygen, nitrogen or argon MW plasma can reduce the strength of the fiber significantly. The tensile

test of CF showed that fiber strength was maximum with seven-minute MW treatment (3.9 GPa) but reduced 26% when subjected to 20 min MW treatment. But the transverse strength of PAN/CF composite increased from 2.20 MPa (untreated) to 4.71 MPa when subjected to 20 min MW treatment. When CF was in touch of polymer matrix, prolong HT resulted improvement of composite strength but the HT time of fiber only should be optimized before using in the composite. Carneiro et al. (1998) [9] pointed about the effect of MW HT on surface modification. CF/PC composites with vapor grown carbon fiber with 5, 10, 20, 30 wt.% CF were fabricated, and 20 wt.% CF/PC composites was treated with oxygen-plasma treated for 3 minutes in a reactor of 70W power. PC with 20 wt.% CF (treated) composite showed 63% positive relative difference in modulus compare to the untreated neat PC. MW HT increased the oxygen content of CF by 15%. Microstructures of heat treated CF showed increased roughness and it improved interfacial bonding between CF and the matrix polymer.

1.2.7 Oven heat treatment of CF reinforced conventional composites

Oven HT for optimal time ensures rough fiber surface, crystallization of polymer and improved polymer fiber bonding. He et al. (2010) [37] observed the impact of heat treatment from 1100 to 1300°C of unidirectional CF reinforced geopolymer composites. The composite was prepared using an ultrasonic-assisted slurry infiltration method. After HT at 1100°C for 90 minutes, flexural strength, work fracture and young modulus of the composite increased 76%, 15%, and 75%, respectively, compare to the untreated composite. The property improvement was explained by the densified and crystallization of matrix and improved interfacial bonding between CF and polymer. Further increase of temperature at 1400°C resulted decrease in strength and brittle behavior on fracture surface was seen. On heating from 900 to 1200°C, 12.4% and 0.9% thermal shrinkage was observed in transverse and radial direction. Matrix expansion was highly hindered

by the shrinkage of CF resulted in formation of evenly distributed oval cracks. On heat treatment at 1100°C, cracks were consistently bridged by CF. But at 1400°C heat treatment, shrinkage-expansion disruption caused by thermal mismatch led to increased crack size and breaking of CF. This led to brittle fracture and lower flexural strength. Note that, the flexural strengths after HT at 1000, 1100, 1200, 1300, 1400°C were 130, 230, 175, 160, and 40 MPa, respectively, and the volume fraction of CF was between 20 to 25%.

The further application of heat treatment has observed for modified and coated CFs and CNTs. Sharma et al. (2011) [38] reinforced epoxy/amine with carbon fiber and with carbon nano fiber (CNF) coated carbon nano tube (CNT). The fiber tows were kept stretched and the matrix was cured at 80°C for 12 hours. The composite was post cured at 120°C and cooled down to normal temperature before characterization. Another set of CNT/CNF coated reinforcement was cured at 700°C. Tensile strength of neat amine, heat treated CF reinforced amine, and heat-treated CNT/CNF reinforced amine were 70, 350 and 350 MPa, respectively. Most of the work on HT of CF reinforced polymers are the preprocessing heat treatment of fibers before the fabrication of composites. In our study, we are concern about the HT of fabricated CF reinforced polymer (PC) composite. Though the presence of porosity can impact directly on CF-polymer interface.

1.2.8 Heat treatment of CF reinforced 3D printed composites

Where in literature a lot of work of plasma/ MW treatment of polymer composites can be found, no such treatment can be found to strengthening bonding between reinforcement and matrix of 3D printed composites. Few works on oven HT can be found for FDM parts and curing of stereolithography (SL) parts. Mori et al. (2014) [39] fabricated CF reinforced ABS parts using a die-less forming process by sandwiching CF by the lower and upper plastic plates fabricated by 3D printing. CF was placed on the top of the lower part. After that, the upper part was printed on

the lower plate-CF surface and the part was placed in a drying oven for heat treatment for 15 mins. Nozzle temperature during printing was varied in between 175 to 190°C and specimen dimension was 42 mm (between two necks) × 19 mm × 6 mm. The volume percentage of CF in the parallel sections of the static and fatigue specimens were 1.4% and 1.6%, respectively. Result showed that specimens with and without heat treatment showed the tensile strength of 0.85 and 0.45 KN, respectively. Fatigue results at 10^7 cycles showed that, specimens with and without HT sustained maximum tensile force of 0.58 KN and 0.25 KN, respectively, resulting in a 135% improvement of tensile property (load). Torres et al. (2015) [40] fabricated 3D printed PLA parts using a commercially available FDM. The specification for printed cylindrical torsional part was 100 mm × 7.6 mm. The printed part was heat treated in an oven at 100°C and annealing was done to improve uniformity of the microstructure, relieve stress and improve strength of PLA parts. For neat polymer specimens, heat treatment helps to increase both crystallinity and secondary bonds. The author reported that post annealing treatment between 30 to 60 min at annealing temperature 80°C improved flexural modulus, strength and heat deflection temperature (HDT) significantly with prolong HT. But HT over 60 min didn't show any increase of strength property. Torsion tests showed specimens under 60 min heat treatment (44 MPa) at 100°C showed an improvement of 69% shear strength of than neat PLA specimen without heat treatment (26 MPa). Microstructure of specimen subjected to 20 min HT showed shrinkage of individual strands and the color of outer perimeter of strand also changed reflecting the fact of heat-induced crystallization of PLA.

In literature, no work has found on the post processing microwave of FDM printed parts, but few works on post-curing of 3D printed parts produced by stereolithography can be found. Salmoria et al. (2008) [41] observed that heat treatment of green specimens built with 0.1 mm hatch spacing helps to minimize material anisotropy. In that work, epoxy based DSM SOMOS

7110 SL resin was used with necessary initiators and additives. Post curing was done in a 700W microwave oven for 4 mins. MW post cured parts (42 MPa) showed an increase of 31% of UTS compared to green part without any HT (32 MPa). David Espalin (2012) [42] developed a novel multi-material fabrication process with a shell and core configuration. A hollow cylindrical pressure vessel was created where core material was covered by shell material. The material of shell and core was PC and ABS and the printed multi-material was subjected to HT at 160°C for two hours in an oven. Note that, the glass transition temperature of PC and ABS are ~147°C and ~105°C, respectively. The UTS of PC-ABS heat treated and untreated parts were 30 and 24 MPa. Results showed that heat treated specimen showed an increase of 25% and 18% in tensile strength and modulus of elasticity, respectively. Knoop et al. (2015) correlated the effect of heat treatment and printing quality by testing melt volume rate of polyamide 12 (PA 12). Two different HT temperatures were implemented for the polymer at 235 and 275°C for 300 sec. Melt volume rate showed inversely proportional relationship with viscosity. MVR of PA 12 polymer at 235 and 275°C was 35 and 205 cm^3/10min showing a rise of 485%. Though any stress property wasn't mentioned that can distinguish the effect of HT at 235 and 275°C, it was stated that with reduced viscosity rate of polymers after HT, specimen showed reduction of internal stress and reduced recrystallization. So, the literature shows enough evidence to strengthen 3D printed specimen with HT.

1.3 Motivation

The growing commercialization of FDM parts due to its ability to fabricate complex shaped geometries with holes, and contours, urges the need of strengthening the part, to be used in automotive, aerospace and structural applications. The strength of material extruded part is not

competitive compare to the injection molding, screw extrusion and other conventional methods. In literature, a lot of work can be found where CF was used to reinforce polymers but only a very little work has been done of continuous carbon fiber reinforced 3D printed polymers. Another common thing for conventional fabrication is the improvement of strength properties by heat treatment. To authors' best knowledge, no work on HT of 3D printed composites have been done to increase material property. Three hypotheses inspired the whole work to improve production grade materials for vast applications mentioned above. Firstly, embedding CF in 3D printed polycarbonate (PC) polymer will increase the strength as the Viogt model based on constant strain and Hooke's law stated. Secondly, embedding of CF in FDM printed PC parts without any cavity will create a disturbance in the printing process and the extra material will help to decrease porosity and will improve strength. Finally, it is hypothesized that three different heat treatments; water boiled, oven and microwave heat treatment, will improve the bonding between CF and PC and that may result in improved tensile and flexural strengths.

1.4 Thesis Objectives

There are five objectives for the thesis and listed as follows:

1. Introduction of a novel technique to embed carbon fiber (CF) in FDM printed polycarbonate
2. Design a heat application system that ensures improved bonding between CF and adjacent polymer surface
3. Evaluate a process to decrease porosity by introducing carbon fiber without any cavity as a disturbance in the printing process

4. Implementation of three heat treatment processes (water boiled, oven, and microwave) to utilize the wave absorption property of CF for improved bonding
5. Improving strength of material extrusion 3D printed parts with and without heat treatment

1.5 Thesis Outline

The subsequent thesis has five chapters. Chapter 1 is composed of the evaluation of CF reinforced conventional composites and the effect of oven, and microwave treatment on the composites explaining how CF helps to improve strength with its higher wave absorption property. The chapter also summarizes the works available on fiber reinforced 3D printed polymers and the strength property of the specimens. Chapter 2 represents abstract of the major two parts of this work which are also the part of two submitted journal papers. Chapter 3 is the entire work on reinforcement of material extrusion PC with CF. Chapter 4 shows the impact of HT application to achieve higher tensile yield strength of 3D printed parts to equal the strength obtained from conventional injection molding process and a portion of it describes the flexural strength property.

References

[1] N. Odagiri, H. Kishi and M. Yamashita, "Development of TORAYCA prepreg P2302 carbon fiber reinforced plastic for aircraft primary structural materials," *Advanced Composite Materials,* vol. 5, *(3),* pp. 249-254, 1996.

[2] S. Bose *et al*, "Pore size and pore volume effects on alumina and TCP ceramic scaffolds," *Materials Science and Engineering: C,* vol. 23, *(4),* pp. 479-486, 2003.

[3] S. Kalia, B. Kaith and I. Kaur, "Pretreatments of natural fibers and their application as reinforcing material in polymer composites—a review," *Polymer Engineering & Science,* vol. 49, *(7),* pp. 1253-1272, 2009.

[4] S. Fu *et al*, "Tensile properties of short-glass-fiber-and short-carbon-fiber-reinforced polypropylene composites," *Composites Part A: Applied Science and Manufacturing,* vol. 31, *(10),* pp. 1117-1125, 2000.

[5] G. Williams, R. Trask and I. Bond, "A self-healing carbon fibre reinforced polymer for aerospace applications," *Composites Part A: Applied Science and Manufacturing,* vol. 38, *(6),* pp. 1525-1532, 2007.

[6] X. Lan *et al*, "Fiber reinforced shape-memory polymer composite and its application in a deployable hinge," *Smart Mater. Struct.,* vol. 18, *(2),* pp. 024002, 2009.

[7] F. Rezaei *et al*, "Development of short-carbon-fiber-reinforced polypropylene composite for car bonnet," *Polym. Plast. Technol. Eng.,* vol. 47, *(4),* pp. 351-357, 2008.

[8] E. Thostenson and T. Chou, "Microwave processing: fundamentals and applications," *Composites Part A: Applied Science and Manufacturing,* vol. 30, *(9),* pp. 1055-1071, 1999.

[9] O. Carneiro *et al*, "Production and assessment of polycarbonate composites reinforced with vapour-grown carbon fibres," *Composites Sci. Technol.,* vol. 58, *(3-4),* pp. 401-407, 1998.

[10] R. J. Kuriger *et al*, "Processing and characterization of aligned vapor grown carbon fiber reinforced polypropylene," *Composites Part A: Applied Science and Manufacturing,* vol. 33, *(1),* pp. 53-62, 2002.

[11] M. Hashimoto *et al*, "Prediction of tensile strength of discontinuous carbon fiber/polypropylene composite with fiber orientation distribution," *Composites Part A: Applied Science and Manufacturing,* vol. 43, *(10),* pp. 1791-1799, 2012.

[12] X. Tian *et al*, "Interface and performance of 3D printed continuous carbon fiber reinforced PLA composites," *Composites Part A: Applied Science and Manufacturing,* vol. 88, pp. 198-205, 2016.

[13] N. Li, Y. Li and S. Liu, "Rapid prototyping of continuous carbon fiber reinforced polylactic acid composites by 3D printing," *J. Mater. Process. Technol.,* vol. 238, pp. 218-225, 2016.

[14] G. Goh *et al*, "Additive manufacturing in unmanned aerial vehicles (UAVs): challenges and potential," *Aerospace Science and Technology,* vol. 63, pp. 140-151, 2017.

[15] C. Yang *et al*, "3D printing for continuous fiber reinforced thermoplastic composites: mechanism and performance," *Rapid Prototyping Journal,* vol. 23, *(1),* pp. 209-215, 2017.

[16] G. W. Melenka *et al*, "Evaluation and prediction of the tensile properties of continuous fiber-reinforced 3D printed structures," *Composite Structures,* vol. 153, pp. 866-875, 2016.

[17] F. Ning *et al*, "Additive manufacturing of carbon fiber reinforced thermoplastic composites using fused deposition modeling," *Composites Part B: Engineering,* vol. 80, pp. 369-378, 2015.

[18] H. L. Tekinalp *et al*, "Highly oriented carbon fiber–polymer composites via additive manufacturing," *Composites Sci. Technol.,* vol. 105, pp. 144-150, 2014.

[19] M. Shofner *et al*, "Single wall nanotube and vapor grown carbon fiber reinforced polymers processed by extrusion freeform fabrication," *Composites Part A: Applied Science and Manufacturing,* vol. 34, *(12),* pp. 1207-1217, 2003.

[20] Q. Sun *et al*, "Effect of processing conditions on the bonding quality of FDM polymer filaments," *Rapid Prototyping Journal,* vol. 14, *(2),* pp. 72-80, 2008.

[21] A. K. Sood, R. K. Ohdar and S. S. Mahapatra, "Parametric appraisal of mechanical property of fused deposition modelling processed parts," *Mater Des,* vol. 31, *(1),* pp. 287-295, 2010.

[22] S. Ahn *et al*, "Anisotropic material properties of fused deposition modeling ABS," *Rapid Prototyping Journal,* vol. 8, *(4),* pp. 248-257, 2002.

[23] B. Lee, J. Abdullah and Z. Khan, "Optimization of rapid prototyping parameters for production of flexible ABS object," *J. Mater. Process. Technol.,* vol. 169, *(1),* pp. 54-61, 2005.

[24] P. K. Gurrala and S. P. Regalla, "Multi-objective optimisation of strength and volumetric shrinkage of FDM parts: a multi-objective optimization scheme is used to optimize the strength

and volumetric shrinkage of FDM parts considering different process parameters," *Virtual and Physical Prototyping,* vol. 9, *(2),* pp. 127-138, 2014.

[25] Q. Sun, "Bond formation between polymer filaments in fused deposition modeling process," 2005.

[26] L. D. Blecha *et al*, "Targeted mechanical properties for optimal fluid motion inside artificial bone substitutes," *Journal of Orthopaedic Research,* vol. 27, *(8),* pp. 1082-1087, 2009.

[27] S. J. Kalita *et al*, "Development of controlled porosity polymer-ceramic composite scaffolds via fused deposition modeling," *Materials Science and Engineering: C,* vol. 23, *(5),* pp. 611-620, 2003.

[28] K. Chin Ang *et al*, "Investigation of the mechanical properties and porosity relationships in fused deposition modelling-fabricated porous structures," *Rapid Prototyping Journal,* vol. 12, *(2),* pp. 100-105, 2006.

[29] R. Pennington, N. Hoekstra and J. Newcomer, "Significant factors in the dimensional accuracy of fused deposition modelling," *Proc. Inst. Mech. Eng. Part E J. Process Mech. Eng.,* vol. 219, *(1),* pp. 89-92, 2005.

[30] Q. Dao *et al*, "Calculation of shrinkage compensation factors for rapid prototyping (FDM 1650)," *Computer Applications in Engineering Education,* vol. 7, *(3),* pp. 186-195, 1999.

[31] N. Volpato, J. Aguiomar Foggiatto and D. Coradini Schwarz, "The influence of support base on FDM accuracy in Z," *Rapid Prototyping Journal,* vol. 20, *(3),* pp. 182-191, 2014.

[32] L. Xinhua *et al*, "An investigation on distortion of PLA thin-plate part in the FDM process," *The International Journal of Advanced Manufacturing Technology,* vol. 79, *(5-8),* pp. 1117-1126, 2015.

[33] A. Armillotta, M. Bellotti and M. Cavallaro, "Warpage of FDM parts: Experimental tests and analytic model," *Robot. Comput. Integrated Manuf.,* vol. 50, pp. 140-152, 2018.

[34] A. Gregorian *et al*, "Accuracy improvement in rapid prototyping machine (FDM-1650)," in *Solid Freeform Fabrication Proceedings,* 2001, .

[35] R. Li, L. Ye and Y. Mai, "Application of plasma technologies in fibre-reinforced polymer composites: a review of recent developments," *Composites Part A: Applied Science and Manufacturing,* vol. 28, *(1),* pp. 73-86, 1997.

[36] D. A. Biro, G. Pleizier and Y. Deslandes, "Application of the microbond technique. IV. Improved fiber–matrix adhesion by RF plasma treatment of organic fibers," *J Appl Polym Sci,* vol. 47, *(5),* pp. 883-894, 1993.

[37] P. He *et al*, "Effects of high-temperature heat treatment on the mechanical properties of unidirectional carbon fiber reinforced geopolymer composites," *Ceram. Int.,* vol. 36, *(4),* pp. 1447-1453, 2010.

[38] S. Sharma and S. Lakkad, "Effect of CNTs growth on carbon fibers on the tensile strength of CNTs grown carbon fiber-reinforced polymer matrix composites," *Composites Part A: Applied Science and Manufacturing,* vol. 42, *(1),* pp. 8-15, 2011.

[39] K. Mori, T. Maeno and Y. Nakagawa, "Dieless forming of carbon fibre reinforced plastic parts using 3D printer," *Procedia Engineering,* vol. 81, pp. 1595-1600, 2014.

[40] J. Torres *et al*, "Mechanical property optimization of FDM PLA in shear with multiple objectives," *Jom,* vol. 67, *(5),* pp. 1183-1193, 2015.

[41] G. Salmoria *et al*, "Evaluation of post-curing and laser manufacturing parameters on the properties of SOMOS 7110 photosensitive resin used in stereolithography," *Mater Des,* vol. 30, *(3),* pp. 758-763, 2009.

[42] D. Espalin Jr, *Development of a Multi-Material, Multi-Technology FDM System for Process Improvement Experimentation.* 2012.

[43] D. ASTM, "638-03: Standard Test Method for Tensile Properties of Plastics," *Current Edition Approved Apr,* vol. 1, pp. 1-16, 2008.

[44] E. Thostenson and T. Chou, "Microwave processing: fundamentals and applications," *Composites Part A: Applied Science and Manufacturing,* vol. 30, *(9),* pp. 1055-1071, 1999.

Chapter 2: Abstract of Submitted Journal Papers

2.1 Part 1

Chapter 3

Reinforcement of material extrusion 3D printed polycarbonate using continuous carbon fiber bundles

Abstract

Additive manufacturing (AM) technologies are capable of fabricating custom parts with complex geometrical shapes and contours in a short period of time, relative to traditional fabrication processes that require several post processing steps such as machining and stamping. Material extrusion AM, known commercially as Fused Deposition Modeling (FDM) technology, is a widely used polymer AM process, however, the effects of inherent porosity on mechanical strength continues to be researched to identify strength improvement solutions. To address the effect of porosity and layer adhesion on mechanical properties (which can sometimes result in 27-35% lower ultimate tensile strength when compared to plastic injection molding), an approach was employed to reinforce 3D printed polycarbonate (PC) parts with continuous carbon fiber (CF) bundles. ASTM D638 Type I specimens were fabricated with printing interruptions to manually place and embed CF bundles. Specimens contained either one, two, or three layers of embedded CF bundles. Results demonstrated a maximum of 77% increase in tensile yield strength when PC was reinforced with three CF bundles, and from microstructures, multiple regions were found with zero porosity due to the CF inclusion.

2.2 Part 2

Chapter 4

Post processing heat treatment of material extrusion 3D printed polycarbonate parts reinforced with carbon fiber for improved tensile and flexural strength properties

Abstract

The ever increasing popularity of material extrusion additive manufacturing technology for fabricating complex geometric shaped parts demands strong load bearing capacity for structural and mechanical integrity. In layer-by-layer, manufacturing process, the presence of porosity and insufficient adhesion among layers are the reasons behind lower strength. In traditional manufacturing process of polymers, strength property has been significantly improved with the inclusion of fibers and heat treatment which wasn't considered for 3D printed specimens before this work. In the current study, a special technique was used to fabricate carbon fiber (CF) reinforced 3D printed ASTM D638 Type I and ASTM D790 standard polycarbonate (PC) parts. Four different sets of samples were printed: PC with no CF, one, two, and, three CF bundles and the specimens were subjected to three different heat treatment processes: boiled water, oven (at 115C), and microwave heat treatment for an hour. Microwave treated PC parts with three bundles CF showed 122% increase in tensile yield strength and 20.5% increase in flexural strength than neat PC parts without CF. Porosity reduced significantly and from micrograph, reduction of porosity was due to the disturbance created by CF and the property improved with the increased number of CF bundles rather than the volume fraction.

Chapter 3: Reinforcement of Material Extrusion 3d Printed Polycarbonate using Continuous Carbon Fiber Bundles

3.1 Introduction

Parts fabricated using material extrusion additive manufacturing (AM) and seeking higher levels of structural integrity or functionality are most often filled using either continuous fibers or chopped fibers. Of the available literature, the majority discuss the use of filaments composed of a thermoplastic matrix filled with short fibers. Fiber materials include, for example, continuous or short carbon fiber (CF), carbon nanotubes (CNTs), Kevlar, alumina, glass, kenaf, and natural fibers such as bamboo [1], [2]. Tekinalp et al. (2014) [3] improved the load bearing capacity of acrylonitrile butadiene styrene (ABS) by mixing it with short carbon fibers (3.2 mm length) at 220°C in a compounder with a rotor speed of 60 rpm for 13 minutes. Later, the composite was used to prepare filament and specimens were printed using a desktop printer. When compared to printed neat ABS, a 77% increase in tensile strength (from ~35 MPa to ~62 MPa) was reported when using ABS containing 30 wt.% CF. Fabrication of 40 wt.% CF was also attempted during which the extrusion nozzle clogged repeatedly limiting the number of layers that could be printed. Ning et al. (2015) [4] fabricated carbon fiber reinforced polymer (CFRP) filament using ABS plastic pellets and CF powders (powder diameter was 130 μm and 100 μm) by blending at 220°C. Specimens fabricated with a hobby-level printer showed a 25% increase in tensile yield strength (from 34 MPa to 42 MPa) when including 5 wt.% CF. Higher CF loadings were attempted, but porosity plagued samples such that tensile strength decreased when compared to results of the 5 wt.% specimens.

Although few, there are some examples of research where 3D printed thermoplastic parts were reinforced with continuous fibers. Tian et al. (2016) [5] has demonstrated the simultaneous impregnation and extrusion within a material extrusion machine's liquefier. Note that in this approach, the continuous carbon fiber (CF) is fed into the liquefier and exits simultaneously with the thermoplastic melt. This requires the thermoplastic bead and fiber orientation to be the same. One key material property for this process is the matrix melt flow index. In this respect, a higher melt flow index, measured in g/min at a specific temperature, is desired so that the matrix flow can easily infiltrate into and encapsulate the fiber bundles. Flexural test specimens were fabricated using a desktop material extrusion AM machine loaded with polylactide (PLA) and continuous carbon fiber (1k carbon fiber tow). Process parameters were varied to determine their effect on mechanical and physical properties. The varied parameters were liquefier temperature, layer thickness, filament feed rate, hatch spacing, and printing speed. Results from this work showed a fiber content of 27% by weight yielded 335 MPa and 30 GPa for flexural strength and modulus, respectively. For reference, other work has reported flexural strength and modulus of neat PLA as approximately 100 MPa and 3 GPa, respectively [6].

In another example [7], a Mark One commercially-available printer was used to fabricate tensile testing specimens made from nylon. This desktop material extrusion machine also simultaneously deposits thermoplastic and fibers in the same direction. Printing parameters were held constant while the number of concentric rings (or contours) containing the reinforcement was varied to determine the effect on tensile mechanical properties. Results showed an increase in ultimate tensile strength (UTS) from ~5 MPa for neat nylon to ~85 MPa for specimens containing 5 rings of Kevlar (or 10.1% fiber volume fraction). Another approach to introducing continuous carbon fiber reinforcements into thermoplastic parts fabricated with material extrusion is to place

fibers between layers as opposed to within the plastic beads. This method was used by Yao et al. (2017) [8] to fabricate specimens made of PLA and reinforced with 3k, 6k, or 12k carbon fiber tow. The fibers were impregnated with an epoxy resin prior to placing and adhering the bundle to the 3D printed PLA material. When compared to neat PLA, reinforced specimens showed an increase of 70% and 18.7% for tensile strength and flexural strength, respectively, when containing a single 12k CF bundle. In addition, due to the carbon fiber's piezo-resistive behavior, correlations between strain and resistance were drawn for potential applications as integrated sensors.

Regardless of the method for introducing the carbon fiber, whether it is continuous or short, the presence of interfaces is a key driver for failure. That is, the material systems likely fail due to delamination or stress concentrations at the fiber-matrix interface. In a 3D printed part, interfaces are also present between deposited beads, making early failure more likely. Naaman et al. (1991) [9] found that bond shear stress and relative slip controls frictional shear stress between polymers and fibers, which are the major factors behind de-bonding of fibers. Zhang et al. (2017) [10] stated longer embedded length of CNT-CF based hybrid reinforcement absorbed more energy than carbon fiber and showed better bonding with polymers. Another problem of material extrusion 3D printed reinforced specimens is the presence of material warping behavior due to contraction caused by shrinkage and the uneven distribution of powder in succeeding layers [11]. Armillotta et al. (2018) [12] reported that warpage behavior along a bead's length (distance along the bead) and height (distance across layers) is significant compared to warpage along a bead's width. The phenomena increase more than linearly with the bead's length and decreases monotonically with the bead's height. To illustrate the warpage behavior, the authors explained that material after extrusion cools to surrounding air temperature at a considerable thermal gradient causing

contraction of the specimen which is prevented by the platform. However, upon removing specimens the stress is released due to a bending distortion in the opposite direction.

In this work, embedding of continuous CF, as opposed to short fiber, is studied. In comparison to previous work in literature that used desktop or hobby-style printers, the CF is used to reinforce polycarbonate (PC) material as deposited by a production-grade printer with a heated build chamber. In addition, the embedding process was executed without significant use of a tertiary material for adhering the fiber to the matrix. While there are commercially-available filaments and evidence in literature of using tungsten- and short CF-filled PC with material extrusion AM [13], to the authors' knowledge, there is no work present in literature where PC was reinforced with continuous CF. This work contributes manufacturing methods and characterization data for continuous CF reinforced PC fabricated with a production-grade 3D printing process – fused deposition modeling (FDM, Stratasys' trade name for material extrusion). Characterization data is presented for dimensional accuracy, warpage behavior, fiber material bond strength testing, tensile testing, fracture analysis and study of porosity via scanning electron microscopy (SEM), and quantification of the bond strength between the fiber bundle and the encapsulating PC material.

3.2 Materials and Methods

3.2.1 Specimen Fabrication

ASTM D638 [14] Type I specimens were printed in the XYZ orientation [15] using an FDM 400mc (Stratasys, Eden Prairie, MN) material extrusion machine equipped with polycarbonate (PC). The printing parameters included layer height equal to 0.254 mm (0.010 in.), envelope temperature of 145°C, and T16 extrusion tips. a is the schematic of the raster

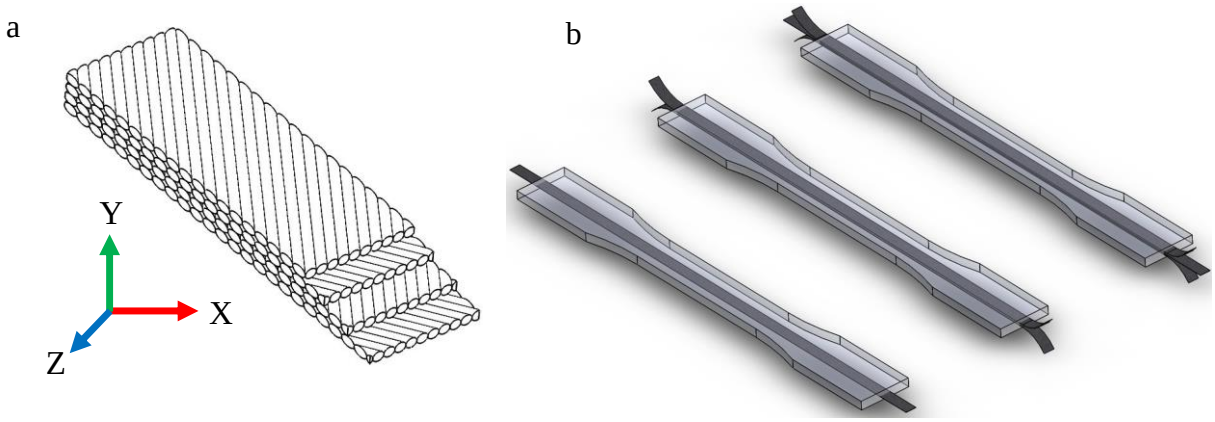

Figure 3. 1 Schematic of 45/-45 raster's direction in FDM part and (b) cartoon of ASTM D638 Type specimens with embedded CF bundles

angle used during printing of tensile testing specimen. Four different sets of samples, each set contained six specimens, were printed, wherein each sample set was printed in individual build sequences. Each specimen was composed of 13 PC layers. The sample sets included neat PC without carbon fiber (CF), PC with one bundle of CF, PC with two bundles of CF, and PC with three bundles of CF. The CF used was unidirectional carbon fabric (4.0 oz) (Fibre Glast Developments Corporation, Brookville, OH) and it was non-woven in nature where in its as-received state contained less than 3% of polyester binder so that maximum possible density of CF can be obtained. The fiber tow making up the fabric included 12,000 filaments per tow (12k). In figure 3. 1b, a cartoon of three different sets of specimens is shown to demonstration the difference between samples in terms of the number of CF bundles. For the introduction of CF within the PC material, a pause in the printing process was programmatically included during which a single CF bundle (i.e., cut section of the fabric) was manually placed and embedded on the planar PC surface. One drop of Permabond 820 high-temperature-adhesive (Permabond engineering adhesive, Pottstown, PA) was used at each end so that the fibers did not move during subsequent PC

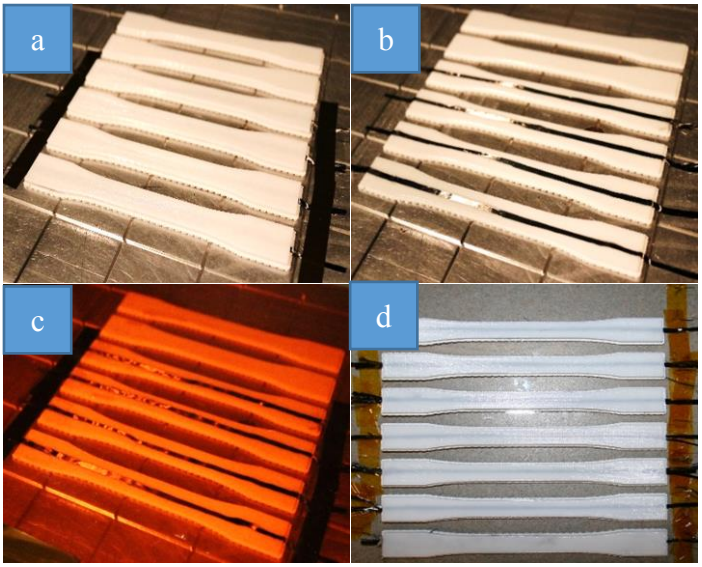

Figure 3. 2 3D printing and CF embedding in PC tensile testing specimen: (a) insertion of CF on PC at pausing of printing process, (b) Kapton film covered specimen for application of heat and pressure, (c) final PC specimen with one bundle embedded CF, and (d) PC specimen with two and three bundles of embedded CF

deposition. After the fibers were placed on the PC substrate, a Kapton film was placed on top of the un-embedded CF bundle and combined heat and pressure was manually applied for approximately 20 seconds. The Kapton film was used to keep any reflowing PC material from creating "mounds" or features that could obstruct subsequent PC deposition by the printer. In addition, it was observed that application of heat and pressure for longer periods of time resulted in undesired bonding between the Kapton film and CF bundle. Therefore, the treatment was limited to 20 seconds. At the conclusion of CF embedding, printing was resumed. Figure 3. 2a shows the steps involved in printing the specimens where Figure 3. 2a shows the CF placement operation on the PC substrate, Figure 3. 2b shows application of Kapton film on embedded surface, and Figure 3. 2c and Figure 3. 2d shows final printed parts with embedded CF. For fabricating PC

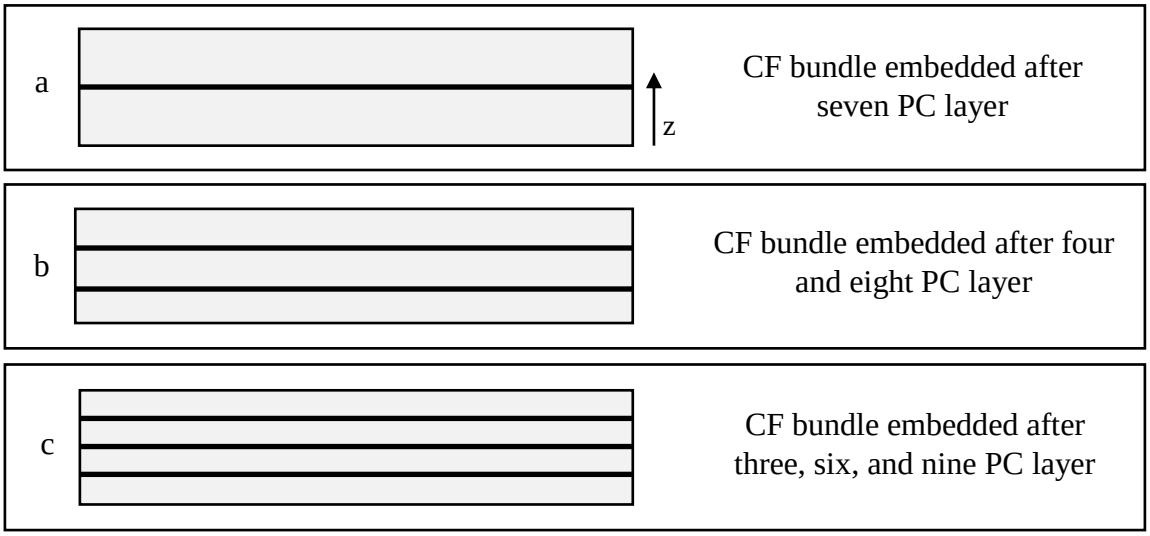

Figure 3. 3 Position of embedded CF along the build direction (z): (a) PC with one bundle of CF, (b) PC with two bundles of CF, and (c) PC with three bundles of CF

with two and three bundles with CF, same procedures were applied. Figure 3. 3 shows a schematic of the specimens noting the build direction (z-axis) and locations of the CF. To make observations of porosity within specimens, a precision cutter (Allied High-Tech Products INC., Rancho Dominguez, CA) was used to cut specimens along the transverse cross-section followed by polishing with a grinding machine (Buehler, Lake Bluff, IL). A Hitachi TM 1000 scanning electron microscope (SEM) (Hitachi High-Technologies Europe GmbH, Germany) was used to observe porosity and CF within the PC material.

3.2.2 Dimensional Accuracy Testing

Dimensional accuracy testing was performed manually using a digital slide caliper. The dimensions (i.e., width and thickness) of all specimens within the four samples were compared with the CAD dimensions. Percent error was calculated based on the formula below.

$$\% \text{ error} = \frac{(\text{measured dimension} - \text{CAD model dimension})}{(\text{CAD model dimension})} \text{ x } 100$$

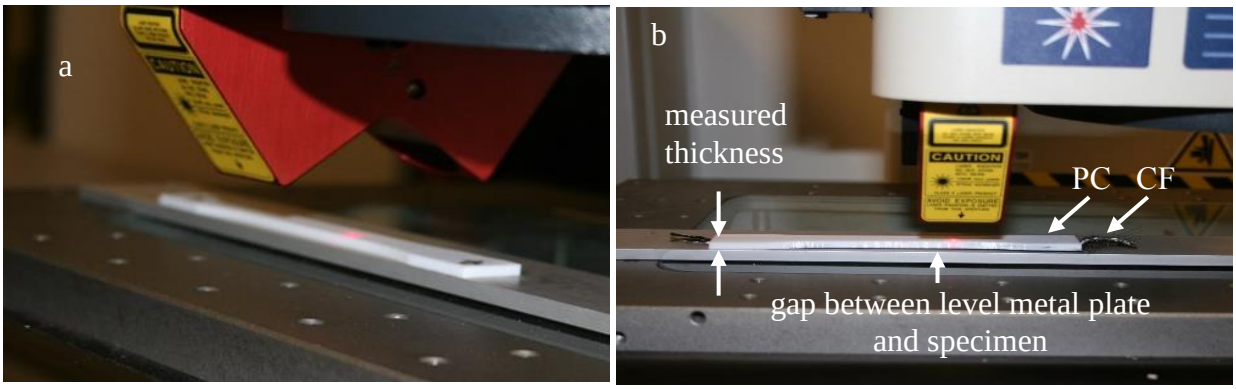

Figure 3. 4 Setup for deformation measurement of 3D printed specimens using laser scanning technology of OGP Smartscope (a) PC with no CF and (b) PC with one bundle of CF

Measurements of the specimen's face relative to a flat plane were collected using the laser scanning capability of a SmartScope Flash 250 (Optical Gaging Products, Rochester, NY). Five specimens were measured for each of the four treatments (no CF, one bundle of CF, two bundles of CF, and three bundles of CF) to quantify the deformation caused by the fabrication process and mismatch in coefficient of thermal expansion (α = 68.4 x 10^{-6} mm/mm/°C for PC, α = -1 x 10^{-6} mm/mm/°C for CF). If the specimen contained no warping (e.g., bending or twisting), then the measured dimension was expected to be equivalent to the thickness of the specimen. Note that figure 3. 4a shows a specimen with no CF where almost no deformation is observable. Figure 3. 4b shows the measuring of a specimen with embedded CF where a noticeable gap between the underlying level metal plate and the specimen indicated a deformed specimen.

3.2.3 Fiber Pull Out Testing

To test the bond between the CF and PC, tensile testing specimens at half-length were printed with a pause at layer seven of total 13 layers at which CF was manually embedded (Figure 3. 5a) using heat and pressure applied over a Kapton film placed above the CF - PC surface. As

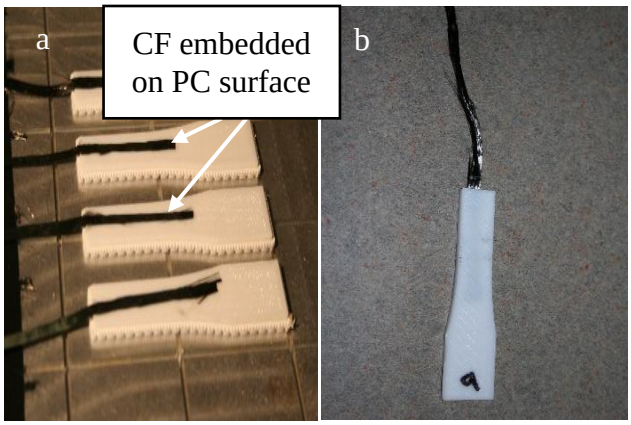

Figure 3. 5 3D printed specimens for fiber pull out test to illustrate bonding behavior between PC and CF (a) CF embedded on PC material, (b) final specimen with fully encapsulated CF

there was no specific standard for a pull out test of CF within 3D printed parts (Figure 3. 5b), ASTM D638 [43] as adopted for this testing. Overall length of the CF was approximately 139.7 mm where 63.5 mm were embedded in the PC material and the remainder was kept outside for proper gripping during pull out testing, which was performed using an Instron 5866 testing machine (Instron, Norwood, MA) with strain rate of 5 mm/min. Before gripping within the testing machine, the unembedded portion of CF was wrapped around a block of PC (not shown in the schematic Figure 3. 6b) and taped to avoid the CF slipping within the grips during testing. Figure 3. 6b shows the schematic diagram of the test setup for fiber pull out test.

3.2.4 Tensile Testing

Tensile testing was carried out according to ASTM D638 using an Instron 5866 tensile testing machine equipped with a 10 KN load cell and a video extensometer while using a strain rate of 5 mm/min on Type I specimens. Figure 3. 6a shows the schematic diagram of tensile test. Prior to testing, printed specimens were kept at ambient temperature and pressure for 2 hours followed by conditioning at 23°C and 50% relative humidity for at least 40 hours according to

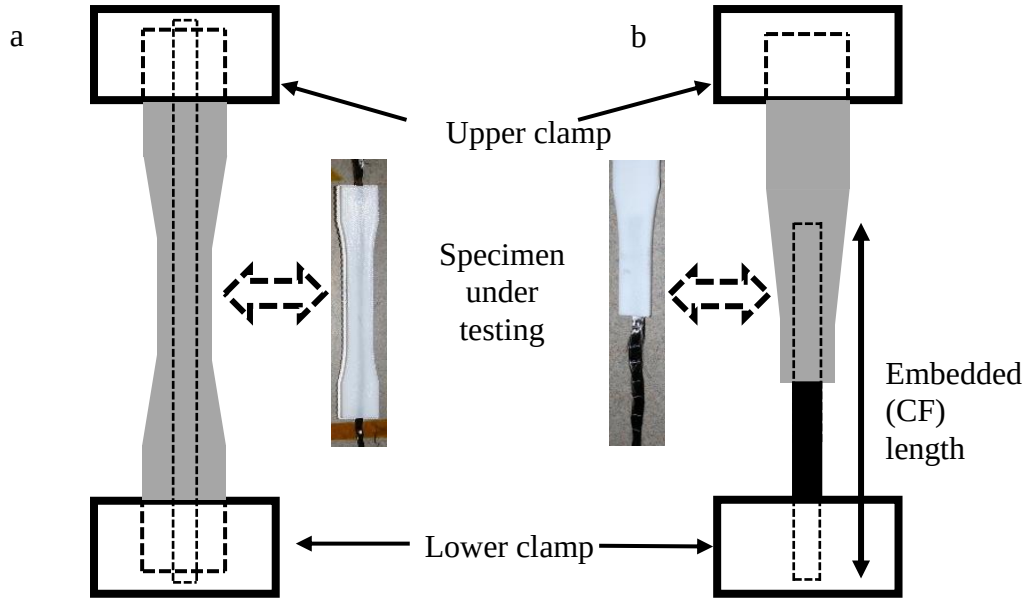

Figure 3. 6 Testing schematic diagram of 3D printed PC specimens with CF: (a) CF-containing specimen under ASTM D638 tensile testing, and (b) modified ASTM D638 Type I geometry under fiber pull-out test wherein one end clamps the PC and the opposite end clamps the CF bundle

ASTM D638 [16]. Yield strength results were collected and used for the analytical calculation of effective theoretical strength. In addition, the modulus, strain at yield, ultimate tensile strength (UTS), and specific UTS were determined. A statistical t-test was performed to test for significance between each sample group at a significance level of 0.05. Fracture surfaces obtained after tensile testing were observed using the Hitachi TM-1000 SEM to find the failure type of the specimen.

3.2.5 Theoretical Strength

The effective theoretical strength was calculated by simultaneously using the Voigt model based on equal strain assumption (commonly referred to as the rule of mixtures model) [17] and Hooke's law shown below where V, E, σ, and ε represent volume fraction, modulus, stress, and

strain, respectively. Experimental values from separately testing PC and CF were used. The width of CF bundle varied from 2.54 mm to 3.81 mm because the fibers were cut manually while the thickness of the CF bundle was 0.152 mm. The mass of the fibers was taken using a digital weight machine, and the mass was divided by the density of CF to get the CF volume.

$$\text{Effective strength, } \sigma = \sigma_{PC}V_{PC} + \sigma_{CF}V_{CF}$$

$$\sigma = E\varepsilon$$

3.3 Results and Discussion

3.3.1 Dimensional Accuracy

The percent error (relative to the CAD dimensions) associated with specimen thickness and width are reported in Figure 3. 7. For the neat thermoplastic specimens, the width and thickness percent errors were 0.5% and 7.4%, respectively. This error has been described by others as having a dependence on, for example, printing orientation, printing position on build sheet, thermal expansion rate of polymer, and cooling rate of polymer [18]. Since the embedded CF had a thickness of 0.152 mm, the expected increase in error was 4.8% (0.152/3.2 x 100) for PC with one bundle CF if the thermoplastic material was completely displaced along the layer stacking direction. However, due to the inherent porosity of material extrusion AM process, the displacement of PC material occurred both along the layer stacking direction and the lateral direction. Intuitively, it was expected that increasing the number of CF bundles along the printing direction would increase thickness error, which occurred and is highlighted by the increased error when comparing one and three CF bundles (8.8% increased to 14% error). The lateral displacement of PC was also noted through the error in specimen width where three CF bundles resulted in an error of 2.9%. One potential solution to reducing the dimensional errors would be through the

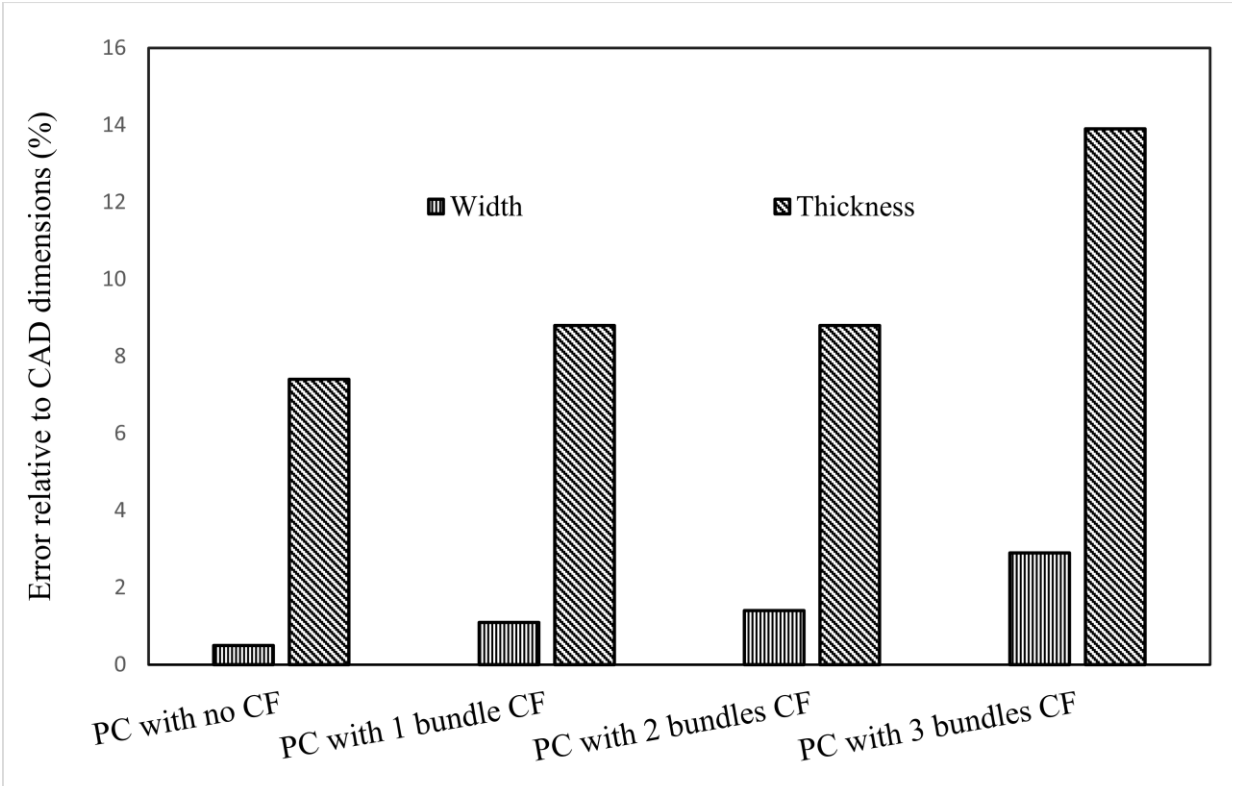

Figure 3. 7 Percentage error of dimensions (when compared to CAD dimensions) for 3D printed PC parts of all samples; note that the values are taken along the middle section of the specimens and dimensions of printed specimens were bigger than the CAD of ASTM D638 Type I dimensions

inclusion of cavities within the PC substrate. The cavities would house the CF bundle to mitigate PC material displacement. Caution must be exercised as this method could also negatively affect adhesion between the CF and PC.

3.3.2 Warp Test

In specimens that contained CF, deformation was more pronounced at the edge furthest from the specimen's centroid. This is often the case even with specimens that do not contain CF. In fact, the neat PC in Figure 3. 8 increases in distance (or warpage) from 3.45 mm at the

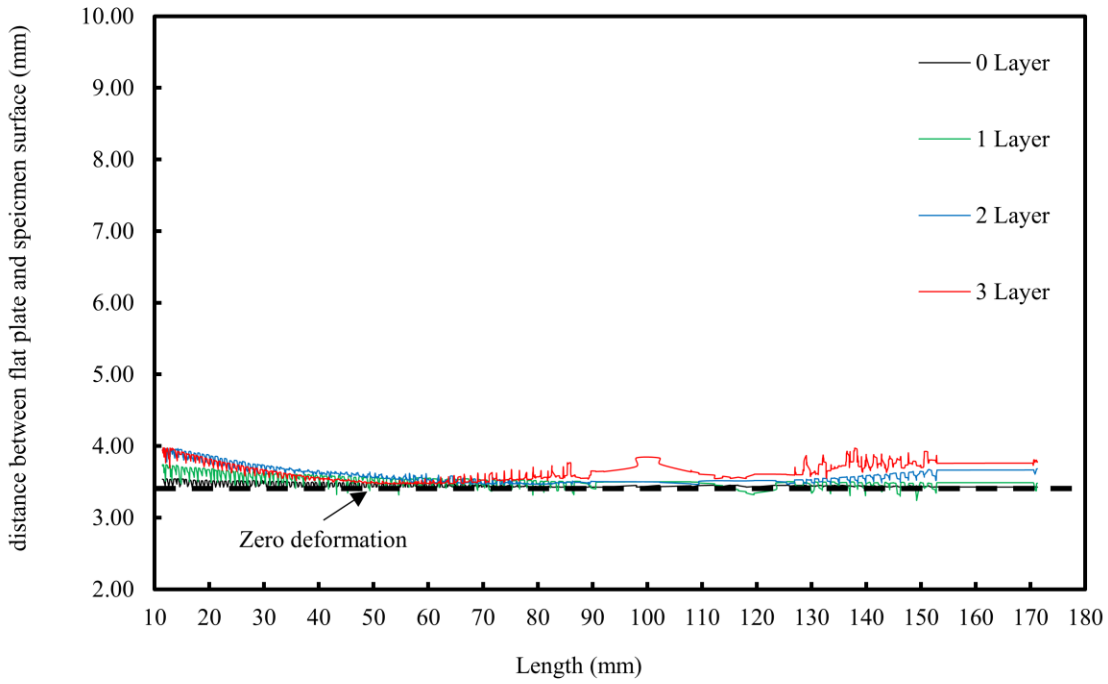

Figure 3. 8 Warp behavior of four different sets of 3D printed samples along Z-axis. Note that, the critical section is shown in inset zoomed view. "Layer" refers to the number of CF bundles embedded in PC

specimen's midpoint to 3.53 mm at the edge. The 3.45 mm distance represents the distance of zero deformation. Therefore, the difference between the highest and lowest measured points for the neat PC was 0.08 mm. Similarly, the specimens containing one, two, and three bundles of CF showed a maximum difference of 0.54 mm, 0.49 mm, and 0.49 mm, respectively. While these measurements do not differentiate between bending and twisting, the trend suggests that deformation occurs with the initial inclusion of CF but increasing CF content does not translate to increased deformation. This could be due to equal amounts of PC material above and below the CF such that bending and twisting on either end of the specimen's thickness is partially balanced. However, the balance of bending and twisting then is expected to develop internal stresses. It

Table 3. 1 Pull out results of 3D printed PC specimens with embedded carbon fiber. Note that specimens were printed with one embedded carbon fiber bundle only

sample No	breaking Strength of CF (N)	comments
1	200	few fibers of CF failed
2	470	CF did not de-bond from the PC specimen, CF failed
3	400	same as specimen 2
4	407	same as specimen 2
5	475	same as specimen 2

should be noted that the balance of bending and twisting as well as internal stresses was not measured.

Another material attribute contributing to warping is the thermal expansion mismatch between PC (α = 68.4 x 10^{-6} mm/mm/°C) and CF (α = -1 x 10^{-6} mm/mm/°C). Upon fabrication completion that occurred at 145°C, the specimens were cooled to room temperature. If thermal contraction and expansion was linear, the PC was expected to contract 1.38 mm [(165 x 68.4 x 10^{-6} x (145-23)] along the specimen's length when cooled from 145°C to 23°C. On the other hand, the CF was expected to expand 0.02 mm along its length when cooled over the same temperature range. Therefore, opposing directions of material movement did not allow PC to move linearly which led to bending and twisting (i.e., warping). In one aspect, the warping of specimens highlights that the bond between the CF and PC is strong such that warping occurs before delamination.

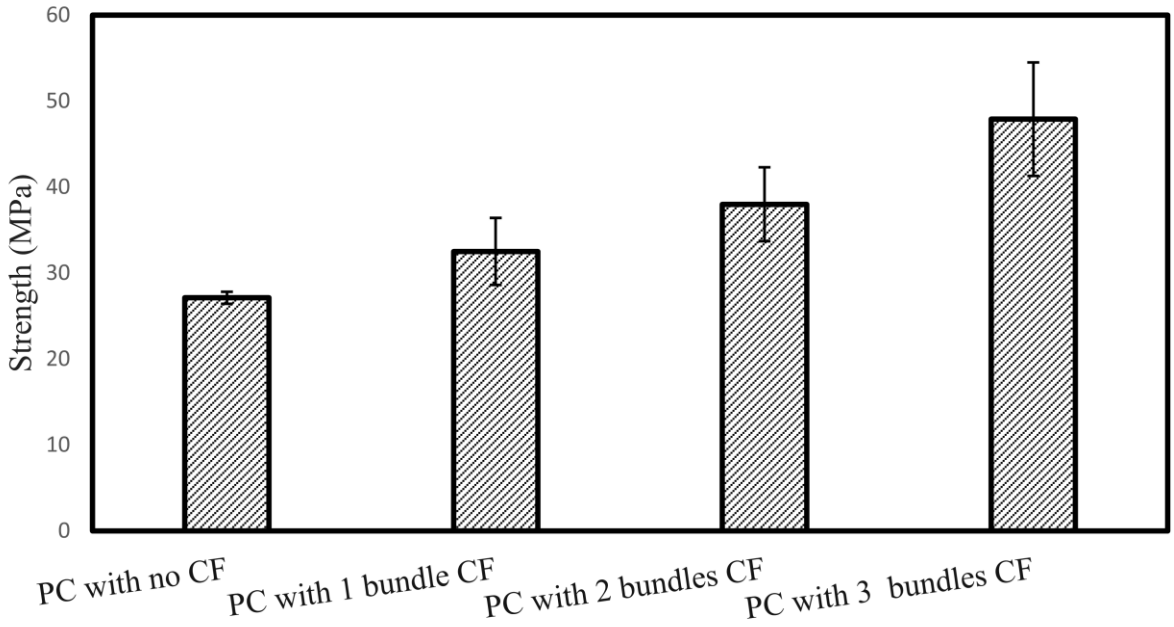

Figure 3. 9 Average tensile results of tensile yield strength of 3D printed specimen for all four sets of samples with sample standard deviation (±σ) (five specimens used for each set)

3.3.3 Fiber Pull out Test

Table 3. 1 shows the load at which the CF bundle failed. Note that all CF bundle failed before the CF-PC interface failed. Specimen 1 failed prematurely at 200 N because the CFs were not all tight during testing leading to only a fraction of the bundle sustaining the tensile load. When considering all other specimens, the maximum bond strength (normalized over the embedded length) between CF and PC was reported as ~7.5 N/mm (475 N/ 63.5 mm). Note that this strength was limited by failure of the carbon fibers and not the interface. Since the fibers failed before the interface, the bond strength is not fully characterized. It is expected that the CF-PC bond strength is higher than 7.5 N/mm.

Table 3. 2 t-test results of average tensile results of tensile yield strength comparing all sets

sample 1	sample 2	t statistical	t critical	p-value (one tail)
PC with no CF	PC with 1 bundle CF	3.04	1.85	0.008
PC with no CF	PC with 2 bundles CF	5.64	1.86	0.0002
PC with no CF	PC with 3 bundles CF	7.02	1.86	0.00005
PC with 1 bundle CF	PC with 2 bundles CF	2.12	1.86	0.03
PC with 1 bundles CF	PC with 3 bundles CF	4.49	1.86	0.001
PC with 2 bundles CF	PC with 3 bundles CF	2.82	1.86	0.01

3.3.4 Tensile Testing

Figure 3. 9 shows mean tensile yield strength for neat PC specimens and those containing embedded CF bundles. In general, the yield strength increased with the number of embedded CF bundles. Note that the coefficient of variation increased from the neat PC (0.025%) to that of PC with embedded CF bundles (0.12% – 0.14%). This increase in variation is attributed to the manual CF embedding process. Even so, the coefficient of variation was still relatively low for specimens with embedded CF. PC with three bundles of CF resulted in a 77% increase of tensile yield strength compared to specimens without CF. Tensile yield strength of injection molded PC varies from 58 MPa to 63 MPa, which is higher than the 3D printed neat PC (average 27 MPa); and inclusion of CF increased strength to 48 MPa. One reason behind the low increase in strength was

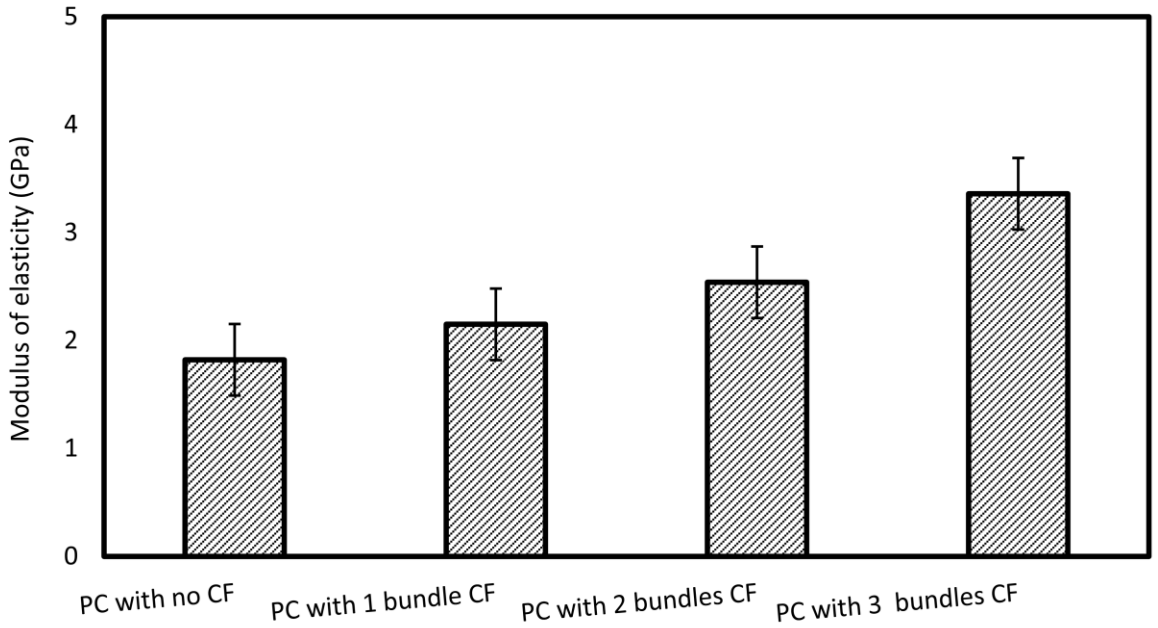

Figure 3. 10 Results of modulus of elasticity of 3D printed specimens of all different sets of samples with sample standard deviation (±σ) (five specimens used for each set)

due to the low volume fraction of CF (0.01 to 0.04) in the PC-CF specimens. In most published composites work, researchers suggest using 25%-50% reinforcement for higher mechanical strength [19]. Table 3. 2 shows that the tensile yield strength obtained with all the samples (i.e., PC with no CF, PC with one CF bundle, two CF bundles, and three CF bundles) were significantly different (p-value < 0.05) when compared to one another. Therefore, the null hypothesis that there is no difference in the ultimate tensile strength between each group is rejected.

Table 3. 3 lists the values that were used with the Voigt model and Hooke's law to determine the theoretical effective strength. The PC strength was recorded at a strain level of 0.002 since the CF, when tested independently, transitioned from linear to plastic deformation at that strain. This ensured that Hooke's law was being employed for both materials in the elastic

Table 3. 3 Comparison of theoretical strength and experimental strength of 3D printed specimens. Note that strength of PC was taken from the same strain rate at which CF failed and the result has error because of porosity and multiple bundles.

sample	CF volume fraction, V_{CF}	strength, σ_{CF} (MPa)	PC volume fraction, V_{PC}	PC strength, σ_{PC} (MPa)	theoretical effective strength (MPa)	experimental strength (MPa)
PC with 1 bundle CF	0.013	3860	0.988	7.5	53.7	32.0
PC with 2 bundles CF	0.025	3860	0.975	7.5	103.8	38.0
PC with 3 bundles CF	0.036	3860	0.964	7.5	146.1	48.0

region. The experimental tensile strength at the elastic yield, for each of the three cases in table 3. 3, were lower than the calculated theoretical effective strength. Several things are suspected to have contributed to the discrepancy: printed specimens had porosity, CF bundles were embedded manually, and inconsistent bonding between adjacent CF and between CF and PC.

Table 3. 4 t-test results (two-sample assuming equal variances) when comparing modulus of elasticity of all samples

sample 1	sample 2	*t* statistical	*t* critical	*p*-value (one tail)
PC with no CF	PC with 1 bundle CF	6.5	1.86	0.0009
PC with no CF	PC with 2 bundles CF	5.2	1.86	0.0004
PC with no CF	PC with 3 bundles CF	6.5	1.86	0.0008
PC with 1 bundle CF	PC with 2 bundles CF	2.7	1.86	0.01
PC with 1 bundles CF	PC with 3 bundles CF	5.1	1.86	0.0004
PC with 2 bundles CF	PC with 3 bundles CF	3.03	1.86	0.008

Figure 3. 10 shows that increased volume fraction of CF resulted in an increase of modulus of elasticity. For all samples, strain varied from 0.9% to 1.85% at the elastic yield point and was around 2% to 5.5% at fracture point. To be more specific, minimum fracture strain was found for PC with 1 bundle CF whereas PC with 3 bundles CF showed maximum strain at fracture.

Table 3. 4 shows results from the two-sample t-test analysis with equal variance for modulus of elasticity. Results showed that modulus of elasticity for all the samples were significantly different (*p*-value <0.05) when compared to one another. Therefore, the null hypothesis that there is no difference in the modulus of elasticity between each group is rejected.From the ratio of obtained tensile yield strength and mass of specimen, specific strength (SS) was measured to illustrate the benefits of embedding CF in PC.

Table 3. 5 Results for specific strength of four different sets of samples

samples	tensile yield strength (MPa)	mass (g)	Specific Strength, SS (MPa/g)
PC with no CF	27.0	9.4	2.9
PC with 1 bundle CF	32.5	9.5	3.4
PC with 2 bundles CF	38.0	9.6	4.0
PC with 3 bundles CF	48.0	9.7	4.9

Table 3. 5 shows that SS increased with increasing bundle of CF (or increasing mass). When considering specimens with three CF bundle, there was an increase of ~3% in mass, which resulted in a 69% increase in SS. Clearly, the increase in mass is well compensated by the increase in strength.

3.3.5 Fractured and polished surface morphology

The fracture surface morphology of selected specimens can be observed in figure 3. 11 where the main characteristic is craze cracking indicative of a mainly brittle fracture mode. The PC specimen with no fiber exhibited multiple crack initiation sites with hackle lines in multiple directions causing angled plane indicating multiple crack propagation fronts (Figure 3. 11a), whereas the PC specimen with one bundle of CF exhibited large fracture surface planes and also possessed a secondary crack emanating from the discontinuity caused by embedding of the carbon fiber (figure 3. 11b). Fracture surface of PC specimens with two bundles of CF (figure 3. 11c)

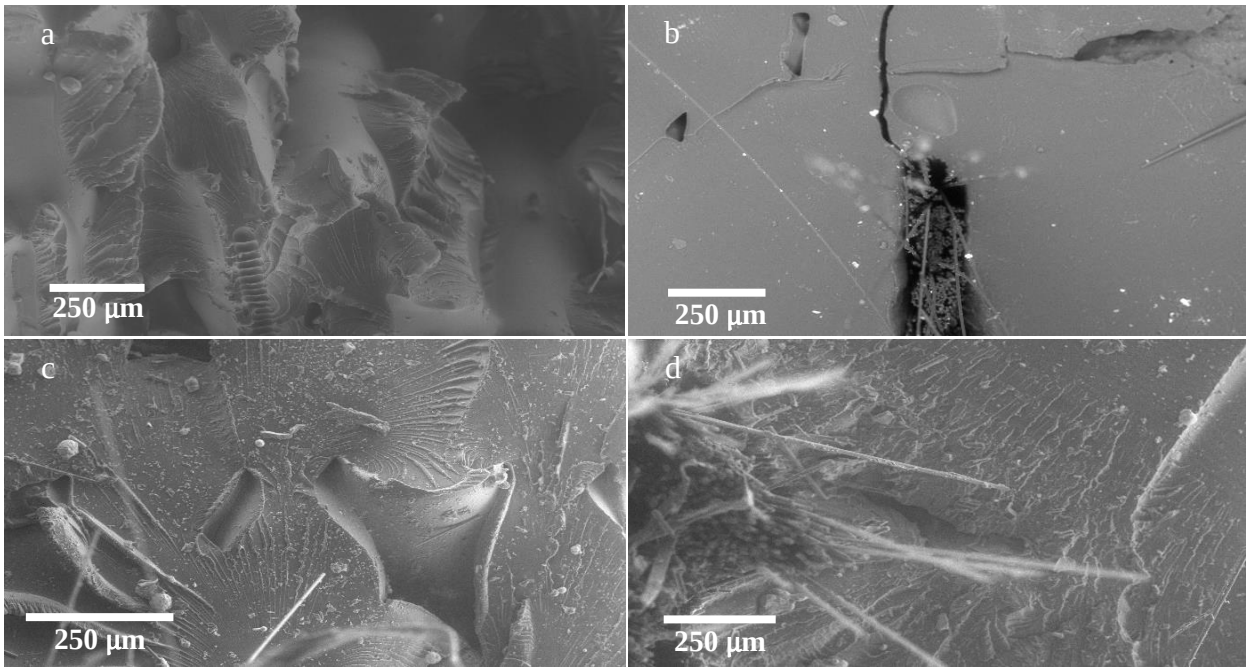

Figure 3. 11 SEM micrographs of tensile testing 3D printed PC specimen fracture surfaces (a) craze cracking is observed for PC with no CF (b) multiple planes with fracture line propagated for PC with one bundle of CF, (c) crack propagation direction for PC with two bundles of CF, and (d) secondary cracks with propagation direction observed for PC with three bundles of CF

shows presence of beach mark which confirmed crack initiated from the inside of the specimen to outside.

PC with three bundles of CF (Figure 3. 11d) shows secondary crack propagation occurred from the disturbance created by the three bundles CF and crack propagated from center to outside.

The scanning electron micrograph in Figure 3. 12a is of the PC surface without any CF where discrete porous behavior can be seen. For PC with one bundle of CF (Figure 3. 12b), the next layer three layers of the embedded surface had no voids which, in this study, is named as Zero Porous (ZP) area. Figure 3. 12c shows the microstructure of PC with two bundles of CF and each layer of CFs contributed to produce void less ZP regions that ended up with six layers (1.53 mm) without any porosity. The electron micrograph of PC with three bundles of CF (Figure 3. 12d)

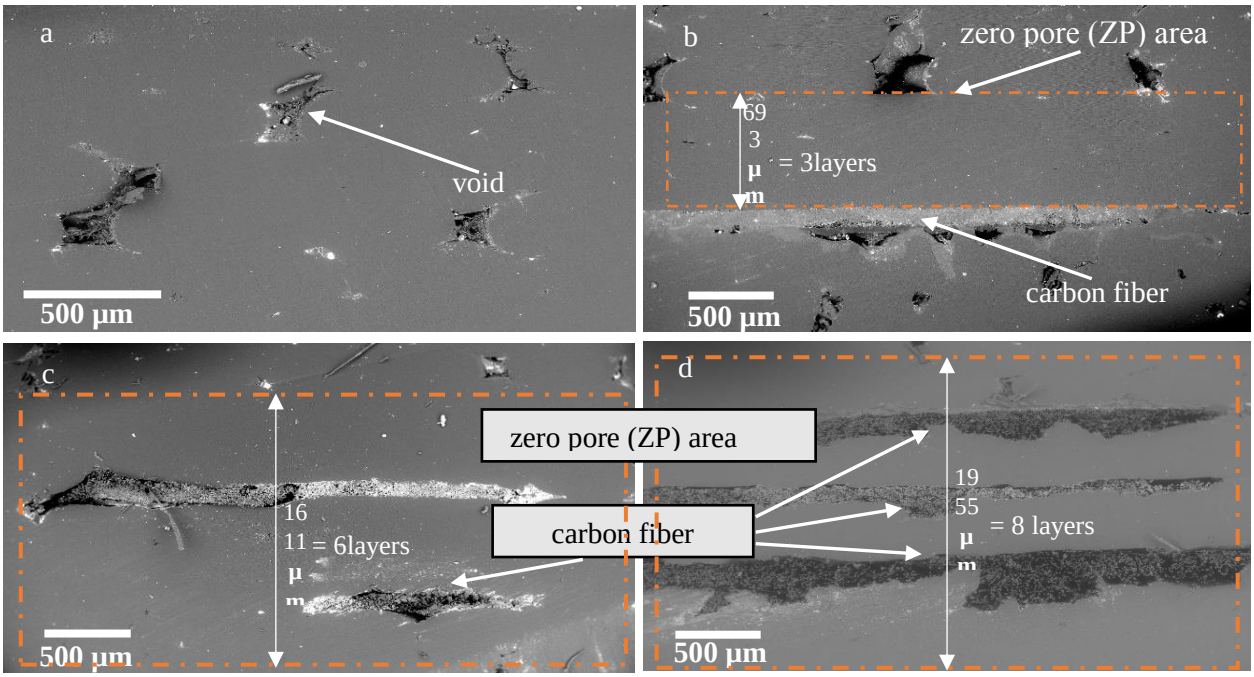

Figure 3. 12 SEM micrographs of polished surface of 3D printed PC specimen along cross section (a) PC with no CF shows larger shaped voids, (b) PC with one bundle CF shows both Zero pore (ZP) area and voids, (c) above 90% of ZP area is found for PC with two bundles and, (d) PC with three bundles of CF showed complete ZP area

showed ZP regions with eight pore-free layers (2.3 mm). The volume fraction of CF (maximum of 0.04 for three bundles) was relatively smaller than the whole PC-CF specimens indicating that a reduction of porosity is not dependent on the volume fraction of CF, but rather, is driven by the number of bundles of CF within the structure. Another notable observation was that for PC with two and three bundles CF, a small region just below the first CF was free of voids; a characteristic that was not observed in the case of PC with one bundle of CF. Therefore, once the total embedded CF bundle thickness is equal (0.31 mm for two bundles CF) or greater (0.46 mm for three bundles CF) than the thickness of one layer (0.254 mm) of printed filament, the phenomena of void less surface appears below the first embedded CF. With the increase in the number of CF bundles, more extruded filaments are spatially displaced, filling any voids that would normally manifest

and the printer tip provides increased pressure downward that helps to remove porosity below the first embedded CF. Additionally, the decrease in voids with an increase in CF material indicates that the CF retains heat allowing for diffusion phenomena to create a more homogeneous polymeric structure.

3.4 Conclusion

To the author's knowledge, this is the first publication wherein continuous CF is used to reinforce PC as dispensed by a production grade material extrusion AM machine. The reinforcement of printed PC with three bundles of CF showed 77% increase of tensile yield strength compared to neat printed PC. Increase of strength was the combined effect of CF reinforcement and reduction of porosity as noted through SEM images. PC with two and three bundles of CF showed regions of zero porosity wherein a maximum of eight layers was found without porosity. The mismatch in thermal expansion coefficients for PC and CF resulted in warping of specimens. Warping was seen with the introduction of CF; however, the warping behavior did not increase with the increase of CF bundle layers. The inclusion of CF into printed PC showed a substantial specific strength increase (from 2.9 MPa/g to 4.9 MPa/g) for a marginal increase in mass (from 9.4g to 9.7 g). Pull-out testing concluded that the adhesion between the CF fabric and PC was stronger than the CF ultimate tensile strength as bundle failed before the CF-PC interface failed.

Acknowledgements

The fabrication and characterization presented here was conducted at The University of Texas at El Paso (UTEP) within the W.M. Keck Center for 3D Innovation (Keck Center) using

equipment developed via a previously funded effort through the National Center for Defense Manufacturing and Machining under the America Makes Program entitled ‘3D Printing Multifunctionality: Additive Manufacturing for Aerospace Applications’ (Project #4030) and based on research sponsored by Air Force Research Laboratory, under agreement number FA8650-12-2-7230. Partial project support was provided by the Mr. and Mrs. MacIntosh Murchison Chair I in Engineering at UTEP (Ryan Wicker). The authors acknowledge the contribution of Leonardo Gutierrez Sierra, Gilberto Siqueiros, Lluvia Herrera, and Mohammad Shojib Hossain for their assistance and support during experimentation.

The views and conclusions contained herein are those of the authors and should not be interpreted as necessarily representing the official policies or endorsements, either expressed or implied, of Air Force Research Laboratory or the U.S. Government. The U.S. Government is authorized to reproduce and distribute reprints for Governmental purposes notwithstanding any copyright notation thereon.

References

[1] Kalia, S., Kaith, B.S. and Kaur, I., 2009. Pretreatments of natural fibers and their application as reinforcing material in polymer composites—a review. *Polymer Engineering & Science*, *49*(7), pp.1253-1272.

[2] Wang, X., Jiang, M., Zhou, Z., Gou, J. and Hui, D., 2017. 3D printing of polymer matrix composites: A review and prospective. *Composites Part B: Engineering*, *110*, pp.442-458.

[3] Tekinalp, H.L., Kunc, V., Velez-Garcia, G.M., Duty, C.E., Love, L.J., Naskar, A.K., Blue, C.A. and Ozcan, S., 2014. Highly oriented carbon fiber–polymer composites via additive manufacturing. *Composites Science and Technology*, *105*, pp.144-150.

[4] Ning, F., Cong, W., Qiu, J., Wei, J. and Wang, S., 2015. Additive manufacturing of carbon fiber reinforced thermoplastic composites using fused deposition modeling. *Composites Part B: Engineering*, *80*, pp.369-378.

[5] Tian, X., Liu, T., Yang, C., Wang, Q. and Li, D., 2016. Interface and performance of 3D printed continuous carbon fiber reinforced PLA composites. *Composites Part A: Applied Science and Manufacturing*, *88*, pp.198-205.

[6] Letcher, T. and Waytashek, M., 2014, November. Material property testing of 3d-printed specimen in PLA on an entry-level 3d printer. In *ASME 2014 International Mechanical Engineering Congress and Exposition* (pp. V02AT02A014-V02AT02A014). American Society of Mechanical Engineers.

[7] Melenka, G.W., Cheung, B.K., Schofield, J.S., Dawson, M.R. and Carey, J.P., 2016. Evaluation and prediction of the tensile properties of continuous fiber-reinforced 3D printed structures. *Composite Structures*, *153*, pp.866-875.

[8] Yao, X., Luan, C., Zhang, D., Lan, L. and Fu, J., 2017. Evaluation of carbon fiber-embedded 3D printed structures for strengthening and structural-health monitoring. *Materials & Design*, *114*, pp.424-432.

[9] Naaman, A.E., Namur, G.G., Alwan, J.M. and Najm, H.S., 1991. Fiber pullout and bond slip. I: Analytical study. *Journal of Structural Engineering*, *117*(9), pp.2769-2790.

[10] Zhang, L., De Greef, N., Kalinka, G., Van Bilzen, B., Locquet, J.P., Verpoest, I. and Seo, J.W., 2017. Carbon nanotube-grafted carbon fiber polymer composites: damage characterization on the micro-scale. *Composites Part B: Engineering*, *126*, pp.202-210.

[11] Giordano, R.A., Wu, B.M., Borland, S.W., Cima, L.G., Sachs, E.M. and Cima, M.J., 1997. Mechanical properties of dense polylactic acid structures fabricated by three dimensional printing. *Journal of Biomaterials Science, Polymer Edition*, *8*(1), pp.63-75.

[12] Armillotta, A., Bellotti, M. and Cavallaro, M., 2018. Warpage of FDM parts: Experimental tests and analytic model. *Robotics and Computer-Integrated Manufacturing*, *50*, pp.140-152.

[13] Shemelya, C.M., Rivera, A., Perez, A.T., Rocha, C., Liang, M., Yu, X., Kief, C., Alexander, D., Stegeman, J., Xin, H. and Wicker, R.B., 2015. Mechanical, electromagnetic, and x-ray shielding characterization of a 3D printable tungsten–polycarbonate polymer matrix composite for space-based applications. *Journal of Electronic Materials*, *44*(8), pp.2598-2607.

[14] D. ASTM, "638-03: Standard Test Method for Tensile Properties of Plastics," *Current Edition Approved Apr,* vol. 1, pp. 1-16, 2008.

[15] ASTM Committee F42 on Additive Manufacturing Technologies and ASTM Committee F42 on Additive Manufacturing Technologies. Subcommittee F42. 91 on Terminology, *Standard Terminology for Additive Manufacturing Technologies.* 2012.

[16] D. ASTM, "618. Standard practice for conditioning plastics for testing," ASTM Standard.ASTM International: West Conshohocken PA, 2008.

[17] Kim, H.S., Hong, S.I. and Kim, S.J., 2001. On the rule of mixtures for predicting the mechanical properties of composites with homogeneously distributed soft and hard particles. Journal of Materials Processing Technology, 112(1), pp.109-113.

[18] Pennington, R.C., Hoekstra, N.L. and Newcomer, J.L., 2005. Significant factors in the dimensional accuracy of fused deposition modelling. Proceedings of the Institution of Mechanical Engineers, Part E: Journal of Process Mechanical Engineering, 219(1), pp.89-92.

[19] Bakis, C.E., Bank, L.C., Brown, V., Cosenza, E., Davalos, J.F., Lesko, J.J., Machida, A., Rizkalla, S.H. and Triantafillou, T.C., 2002. Fiber-reinforced polymer composites for construction—State-of-the-art review. Journal of composites for construction, 6(2), pp.73-87.

Chapter 4: Post Processing Heat Treatment of Material Extrusion 3d Printed Polycarbonate Parts Reinforced with Continuous Carbon Fiber for Improved Tensile and Flexural Strength Properties

4.1 Introduction

Material extrusion 3D printed parts seeking improved strength and load bearing capacity are most often done with embedding either short or continuous fibers. In traditional fabrication process of polymer-based composites, fiber materials, for example, carbon nanotubes (CNTs), continuous or short carbon fiber (CF), glass, natural (bamboo), Kevlar fibers are used [1]. Tekinalp et al. (2014) [2] developed a feedstock for a desktop FDM to print specimen with improved tensile strength and porosity property of 3D printed specimen by mixing short carbon fibers (0.2-0.4 mm) with acrylonitrile-butadine-styrene. An Intelli-Torque Pasti-Corder prep-mixer was used to blend the CF and ABS mixer at 220°C for 13 mins. Four diverse types of blend were produced with 10, 20, 30, and 40 wt.% short CF. Later the blend was used to make filament so that it can be used in FDM for printing specimens. The fourth composite filament with maximum short CF faced problem during printing with clogging in the nozzle and adjustment was done on the printing tip for proper quality printing. End result was found that specimen printed with 40 wt.% short CFs, resulted 115% and 700% increase in tensile strength (didn't mention UTS or yield) and modulus, respectively. Ning et al. (2015) [3] used the same concept to produce filament for which virgin ABS pellets and CF of two different length (150 µm and 100 µm) were used. 3%, 5%, 7.5%, 10%, and 15% short CF was mixed and blend with ABS using a mixer and later a plastic extruder (EB-1, Extrusion Bot Co. Chandler, AZ, USA) at 220°C was used to produce FDM usable filament. ASTM Type V specimen was printed using a desktop FDM printer (Creatr, Leapfrog Co., Alphen

aan den Rijn, Netherlands) and the printed specimen with 5 wt.% CF showed maximum 30% increase in tensile strength and 7.5 wt.% CF content showed 37% increase in modulus of elasticity. The further increase of CF wt.% decreased both the strength and modulus. Zhong et al. (2000) [4] used glass fiber reinforced ABS filaments to print Type I specimen using FDM and maximum tensile strength (didn't mention UTS or yield) found was 58.6 MPa which is higher than the neat ABS specimen (didn't mention the value).

Recent works show that the application of continuous CF is being popular, although, not many literatures on continuous CF reinforced 3D printed polymers are available. Tian et al (2016) [5] developed a novel 3D printed technology to fabricate continuous fiber reinforced thermoplastic composites (CFRTPCs). Continuous CF (1000 fibers in a bundle) and PLA was deposited simultaneously in a self-made desktop material extrusion system. For depositing PLA and CF simultaneously, melting flow index was important to study for proper interfacial impregnation between CF and PLA. Parameters involved with the fabrication process was: printing temperature 180-240°C, layer thickness 0.3-0.8 mm, feed rate of filament 60-160 mm/min. Result showed that PLA specimen with 27% continuous CF showed flexural strength and modulus of 335 MPa and 30 GPa, respectively. Yang et al. (2016) [6] used a desktop FDM printer with the advantage of simultaneous deposition of melting thermoplastic ABS material and continuous hot dipping of CF. The printing parameter included layer thickness of 0.5 mm, extrusion temperature 230°C, envelope temperature 90°C and feed speed 5 mm/s. Results showed that flexural strength and tensile strength of 10 wt.% continuous CF embedded ABS specimen improved to 127 and 147 MPa which is far higher than the neat ABS specimen. Melenka et al. (2016) [7] developed a commercial desktop 3D printer 'Markone' by Mark forged that can print 3D printed specimen with continuous fiber. Markone was used to print continuous ring-shaped Kevlar fiber in nylon material. Four different

samples were printed with zero, two, three, four, and five rings to print ASTM D639-14 Type I specimens. Specimens with two, four and five Kevlar rings reinforced Nylon showed ultimate tensile strength of 32, 58, and 80 MPa respectively. Three different volume fraction of Kevlar fibers (i,e: 4.04, 8.08, and 10.1%) were used to print specimens which resulted modulus of elasticity of 4155.7, 7380.0 and 8992.1 MPa, respectively (less than the theoretical values).

In traditional fabrication process heat treatment (HT) is widely used for strength improvement but additive manufacturing is limited to few oven HTs only. Mori et al. (2014) [8] studied continuous carbon fiber bundle (280 fibers in one bundle) reinforced ABS (wire diameter 1.75 mm) composites under oven HT. The fabrication includes sandwiched CF between lowed and upper 3D printed plastics plates and drying the specimen in an oven for 15 minutes for ensuring better bonding. Though the work didn't distinguish between the strength property of ABS with CF and oven treated ABS with CF, conclusive results showed 400% increase of ultimate tensile strength of oven treated ABS-CF composite (1.5 KN) than neat ABS specimen (0.3 KN). Torres et al. (2015) [9] worked on the processing parameters of FDM printed PLA specimen with heat treatment at 100°C with varying time (0 min, 5 min, and 20 min) where implementation of heat treatment increased mechanical properties slightly, but the ductility property decreased. Note that, samples failed at 25 MPa yield strength (strain rate was 0.2%) without any heat treatment, and specimens with 20 min HT showed yield strength of 42 MPa, an increase of 68% but caused significant loss of ductility. Salmoria et al. (2005) [10] used UV and microwave post cured samples printed by stereolithography technology that resulted improved elastic modulus, tensile strength and ultimate tensile strength properties than the green part. Note that, failure stress of green part was 32 MPa and after micro-wave post curing, strength increased to 42 MPa. Espalin Jr et al. (2012) [11] developed a novel multi-material fabrication method with a shell (PC) and core (ABS)

configuration and HT at 160°C (greater than the glass transition temperature of both shell and core) for 2 hours in an oven, resulted 25% increase in ultimate tensile strength and 18% increase of modulus of elasticity [4].

The molecular interaction with the electromagnetic field helps microwave (MW) to deliver energy to the material. In conventional process, heat is transfer to the material through conduction, convection or radiation but for MW, electromagnetic energy penetrates the material rapidly and converts to thermal energy [12]. In literature, no such work was found on MW treatment of FDM printed parts or composites. But in the traditional fabrication of composites, application of MW became popular because of the improvement of strength. Lee et al. (2014) [13] improved the interfacial bonding and mechanical interlocking between carbon fiber fabric and cyclic butylene terephthalate (CBT) oligomer matrix polymer by microwave plasma treatment. A technology was developed with gas chamber, gas injector, and microwave guide and quartz tube for the treatment. Microwave frequency was 2.45 GHz with 1 KW power capable of discharging Argon plasma. The plasma treated CF (specimen or CF?) was subjected to microwave for 5 min per unit surface area and result showed 436.3% increase in mechanical strength compare to the polymerized CBT matrix. Liu et al (2011) [14] mentioned that CF has the properties of low weight, and low electrical resistivity (10^{-2} ohm cm) which makes it a suitable electromagnetic wave absorptive material and that improves surface modification of polymer-CF when subjected to MW treatment. At -10dB to -20dB, reflection loss of microwave absorption of materials increased 90% to 99% and resulted in increase in absorption of energy.

Material extruded 3D printed polymers regardless of the application with or without embedded fibers, has drawbacks like dimensional inaccuracy, warp behavior etc. Anitha et al. (2001) [15] implies on major parameters i.e. road width, build layer thickness, speed of deposition,

temperature, humidity, wire diameter etc., influence the quality of prototype in FDM. Zeimian et al. (2001) [16] tested the impact of four process variables i.e.: build orientation, layer thickness, road width, interior fill strategy (three fill types were used: solid, part fast, and cross hatch). Three different shaped specimens (i.e.: prism, rectangle and cylinder) were printed using FDM2000 with layer height 0.178mm and result showed maximum accuracy was found for rectangle and minimum for prism. Another major problem of FDM printed specimen is the warpage of specimens after the extrusion because of the cooling of the specimen at surrounded lower temperature. The specimen tries to shrink because of the lower thermal gradient which is prevented by the platform allowing a residual stress in a direction opposite to the build sheet. However, upon removing the specimens the counter residual stress is released due to bending distortion creating convex shaped specimen [17]. In another study, Gregorian et al. (2001) [18] analyzed the inaccuracy of FDM-1650 part showing that build speed and temperature during printing affect part warpage due to exposure of heat. Another drawback of 3D printed specimen is the presence of inconsistent pores that causes the lower strength. Kalita et al. (2003) [19] fabricated polymer-ceramic composite scaffolds by high shear mixing of polypropylene polymer with TCP ceramic. Three different sets of specimens varying 36, 48, and 52% pore volume were prepared, and compression tests showed 34% increase of strength for 36 pore vol.% specimen (12.7 MPa) than specimen with 52% pore vol.(9.5 MPa).

In this work, a special process has been developed for embedding continuous CF in polycarbonate polymer using a production-grade 3D printing process – fused deposition modeling (FDM, Stratasys' trade name for material extrusion) with a heated build chamber. A post processing heat treatment system was also developed for improved strength property. Though, in literature, some oven treatment of FDM printed polymers are available, to the authors' knowledge,

there is no work present in literature where boiling, oven, and microwave heat treatments were applied on continuous CF reinforced 3D printed PC polymers. Another unique part of the study is that the embedding was done without significant use of adhering material. Dimensional inaccuracy, warpage behavior, tensile, and flexural tests were done, and porosity images were studied using an optical microscope for characterization of the specimen.

4.2 Experimental Setup

4.2.1 Specimen preparation

A production grade FDM 400 mc (Stratasys, Eden Prairie, MN) material extrusion machine was used to fabricate polycarbonate (PC) parts reinforced with continuous carbon fiber (CF). The printing parameter consisted: XYZ orientation [20], printing layer height 0.254 mm (0.01 in), extrusion tip T16 and envelope temperature 145°C. Non-woven unidirectional carbon fabric (4.0 oz) was used. The CF (Fibre Glast Developments Corporation, Brookville, OH) contained less than 3% polyester binder and each fabric contained 12000 filaments per tow (12k).

Two different sets of samples were prepared for tensile test and flexural tests. For tensile tests, ASTM D638 [21] Type I specimens of four different sets of samples: PC with no CF, PC with one, two and three bundles of CF, were printed, each set contained 24 specimens and six specimens from each set were subjected to microwave (MW), oven, boiling heat treatment (HT) and another set without HT. The dimension of embedded CF was 165 mm x 3.25mm x 0.15 mm where the width varied (3.2 to 3.5 mm) due to manual cutting of CF. For each separate set of samples, a pause was inserted automatically during the printing process and upon pause, CF was embedded manually, and unembedded part of CF was fixed with the build platform using Kapton tape. During embedding CF, one drop of Permabond 820 high-temperature-adhesive (Permabond

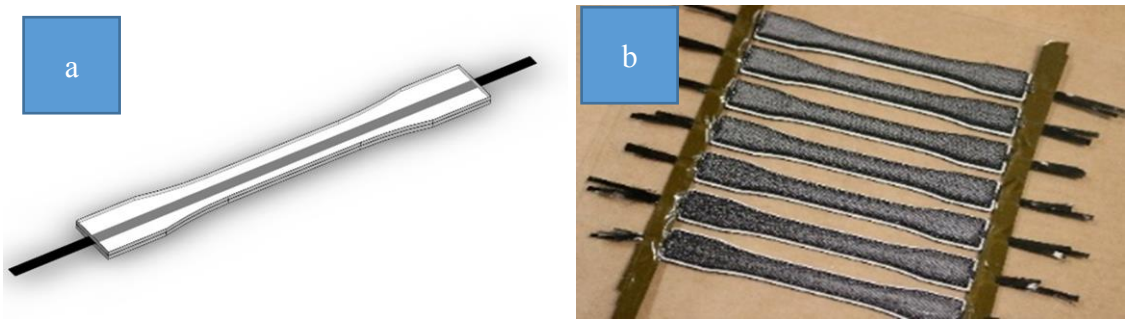

Figure 4. 1 Process involved in fabrication of 3D printed polycarbonate parts with embedded continuous carbon fiber, (a) cartoon and, (b) final parts of D638 Type I tensile specimens

engineering adhesive, Pottstown, PA) was used at each end. For each case, heat and pressure was applied on the CF embedded surface using a Kapton film for 20 seconds to maintain better bonding and to avoid waviness nature of CF. The reason behind choosing 20 seconds for heat application was based on some previous experiments where longer period of heat application was causing undesirable bonding between Kapton film and CF. Printing was paused after certain layers and on the embedded PC- CF surface, heat and pressure were applied, printing was resumed each time after embedding the CF until the final specimen was printed. For PC with one bundle of CF, CF was embedded at seventh layer. Two pauses at fifth and eighth layers were inserted for embedding two CF bundles in PC specimen. For PC with three bundles of CF, CFs were embedded at fourth, seventh and ninth layer. Figure 4. 1a shows the CAD cartoon of PC parts with CF and Figure 4. 1b shows the final set of parts after printing.

For flexural test, ASTM D790 standard specimens were printed using the same procedure. Again, four different sets of samples were printed where each set contained 10 specimens and five from each undergo MW treatment and no HT. Figure 4. 2a shows printing stopped at certain pause

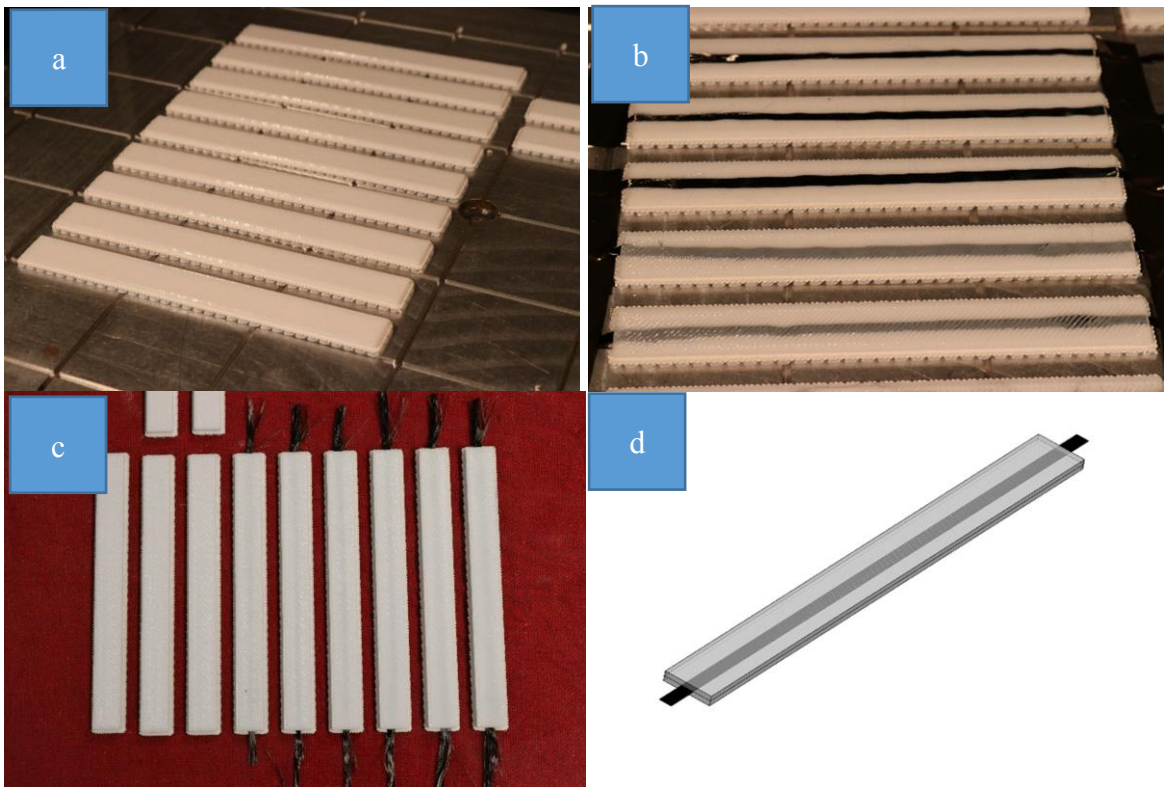

Figure 4. 2 Process involved in fabrication of 3D printed ASTM D790 parts for flexural test: (a) printing paused at certain layers, (b) during the printing of immediate next layer after CE embedment, (c) final parts with and without CF, (d) cartoon of the specimen.

at seventh layer, Figure 4. 2b shows the eighth layer of printing, Figure 4. 2c shows final set after printing and Figure 4. 2d shows the cartoon of specimen. Pauses were inserted at fifth and eighth layers for PC with two CF bundles and at fourth, seventh and ninth layers for PC with three CF bundles.

4.2.2 Post processing operation

The printed sets of PC with zero, one, two, and three CF bundles were subjected to for four different post processing conditions: boiled water, oven heat treatment (HT), microwave (MW) HT and without to any HT. Six specimens from each set (PC with zero, one, two and three CF

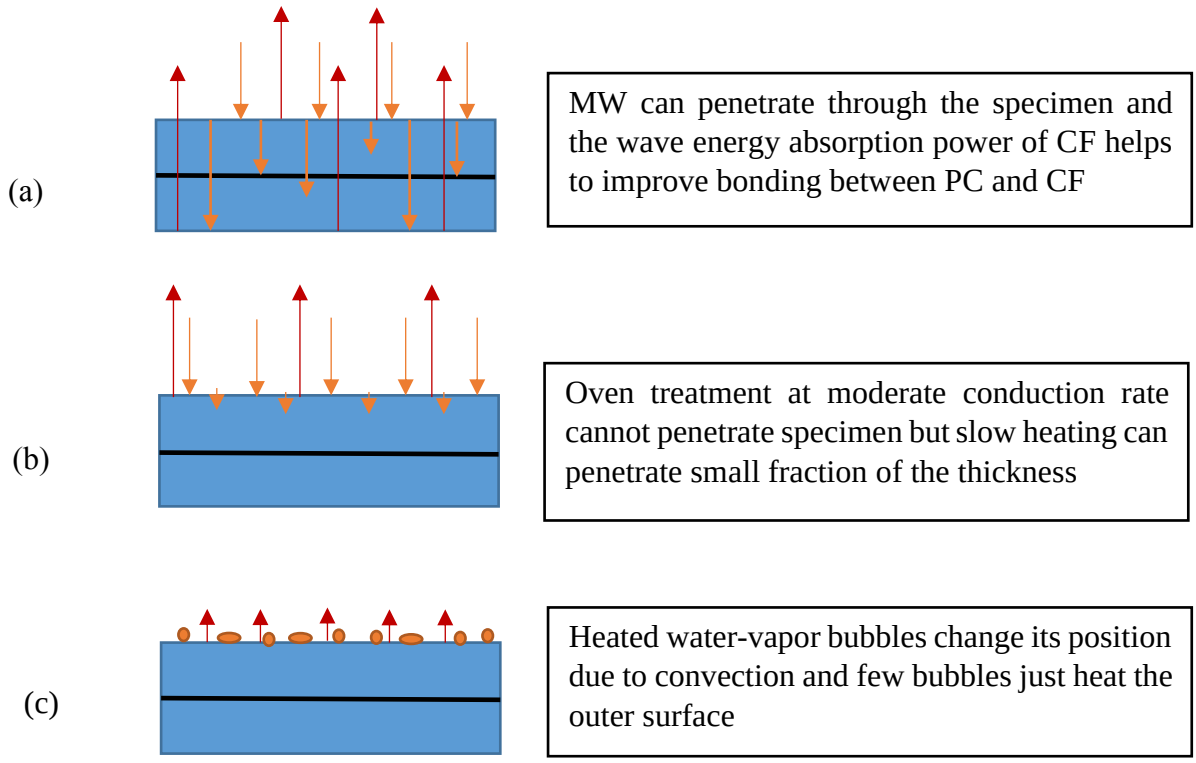

Figure 4. 3 Principal of heat treatments (a) microwave, (b) oven, and (c) water boiled

bundles) was treated in boiled water at 99°C for an hour. A hot plate was used to heat the specimens in boiled water. Another sample containing six specimens, from each set, was placed in a VWR 1370FM oven (Sheldon Manufacturing Inc., Cornelius, OR) for HT at 115°C for an hour. The third set of samples with six specimens from each set was kept in a Sharp R-309YK microwave household oven (One Sharp Plaza, Mahwah, NJ) with the input parameters involved voltage 120V, frequency 60Hz AC, and power1.5 KW. The MW treatment was run for an hour and specimens were dissolved in 1 liter water to avoid the spark caused by the sharp edges of specimens due to the flowing of electrons under MW transmission. Table 4. 1 shows all the types of specimens with specific notations. Figure 4. 3 describes the principals of all HT process pointing out that MW HT can penetrate through the specimen and can react directly with the CF. CF has a high MW absorption property and the heat extracted from the MW helps to soften the PC that surrounds CF

Table 4. 1 Remarks of all 16 types of specimens

Specimens	Heat Treatment (HT)	Notations
PC without CF	No HT	N_0
	Water boiled HT	B_0
	Oven HT	O_0
	MW HT	M_0
PC with one bundle CF	No HT	N_1
	Water boiled HT	B_1
	Oven HT	O_1
	MW HT	M_1
PC with two bundles CF	No HT	N_2
	Water boiled HT	B_2
	Oven HT	O_2
	MW HT	M_2
PC with three bundles CF	No HT	N_3
	Water boiled HT	B_3
	Oven HT	O_3
	MW HT	M_3

and ensures better bonding between PC and CF (Figure 4. 3a). Figure 4. 3b shows that oven HT mainly has impact on the outer surface of specimens, but the presence of porosity may help to heat the inside part of the material. Figure 4. 3c shows the circular shaped water bubbles can't penetrate through the specimen. Note that, boiling HT was done to distinguish if MW treatment of specimens in boiled water was the impact of MW or boiling water. All treatments were done after the immediate fabrication of specimens.

To analyze the microstructure, tensile specimens were cut along cross section using a precision cutter (Allied High-Tech Products INC., Rancho Dominguez, CA) followed by polishing using a grinder machine (Buehler, Lake Bluff, IL). An optical microscope (McBian System, Westlake Village, CA 91361) was used to observe the PC-CF bonding and porosity within the material.

(a) 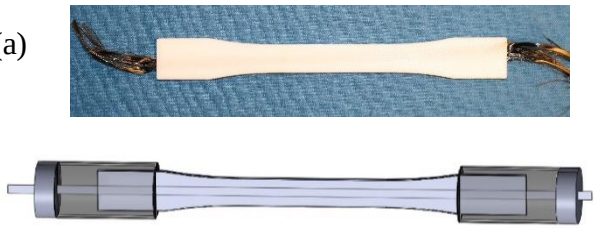 (b) 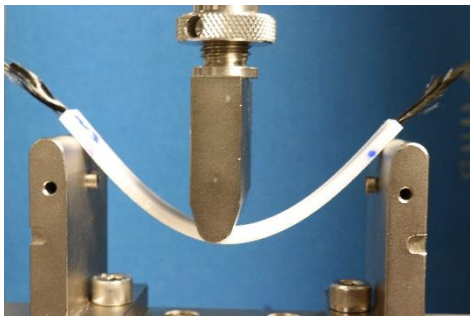

Figure 4. 4 (a) Schematic setup of tensile test with printed specimens and (b) flexural test setup showing maximum bending at 5% flexure strain.

4.2.3 Printing property analysis test

Printed specimens were measured manually along length, width and thickness using a caliper. Measurement of width and thickness were taken from the mid-section of the specimens because of the consideration that change of width at minimum cross section will be maximum and the values were compared with the standard value.

$$\text{percentage inaccuracy} = \frac{(\text{measuremetn from specimen} - \text{standard value from CAD})}{\text{standard value from CAD}}\ x\ 100$$

Printed specimens were scanned by a laser scanner with a SmartScope Flash 250 (Optical Gaging Products, Rochester, NY)) microscope to observe the warp behavior. The specimens were placed on a straight metal plate in a way that makes convex shape with the plate.

4.2.4 Tensile and Flexural Strength test

After HT, specimens were kept in a conditioning environment of 23°C and 50% relative humidity for 40 hours to maintain ASTM D638 standard for tensile testing [22]. An Instron 5866 testing machine (Instron, Norwood, MA) was used to test both tensile and flexural strength. Figure 4. 4 shows the schematic diagram of both the tests.

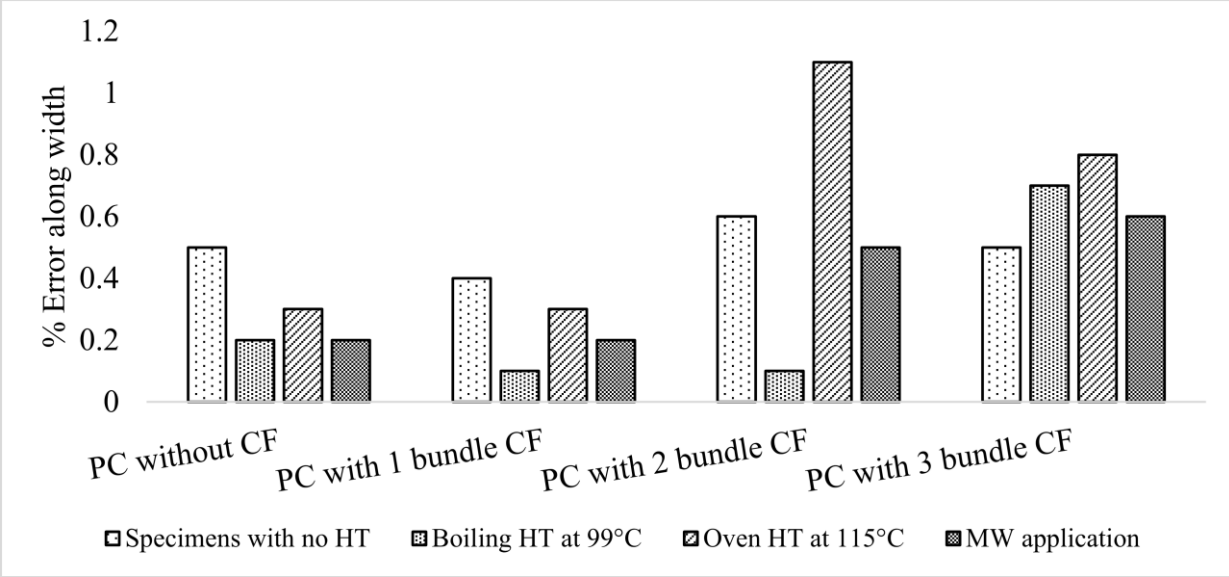

Figure 4. 5 Error percentage of 3D printed PC specimens with and without CF for all specimens under four different post processing heat treatment: along width. Note that no trend was found between inaccuracy and increased number of CF bundle.

4.3 Result and Discussion

4.3.1 Dimensional Inaccuracy

The percent inaccuracy associated with the specimen along width and thickness compared to the CAD dimensions are reported in Figure 4. 5 and Figure 4. 6. Neat thermoplastic specimen showed 0.5% errors along width. Note that, the percent error was relatively low and varied from 0.1% (for boil treated PC with one bundle CF) to 1.1% (for oven treated PC with two bundle CF). Comparing to the width, significant errors were noticed along thickness and varied from 7.1% (for MW treated PC without CF) to 9.7% (for oven treated PC with two bundle CF). It is considerable to have inaccuracy for specimens with CF bundle because of the embedding of CF without any cavity. But for neat PC, 0.5% and 7.4% errors were noticed along width and thickness, respectively. Pennington et al. (2005) [23] mentioned about factors that affects the accuracy of

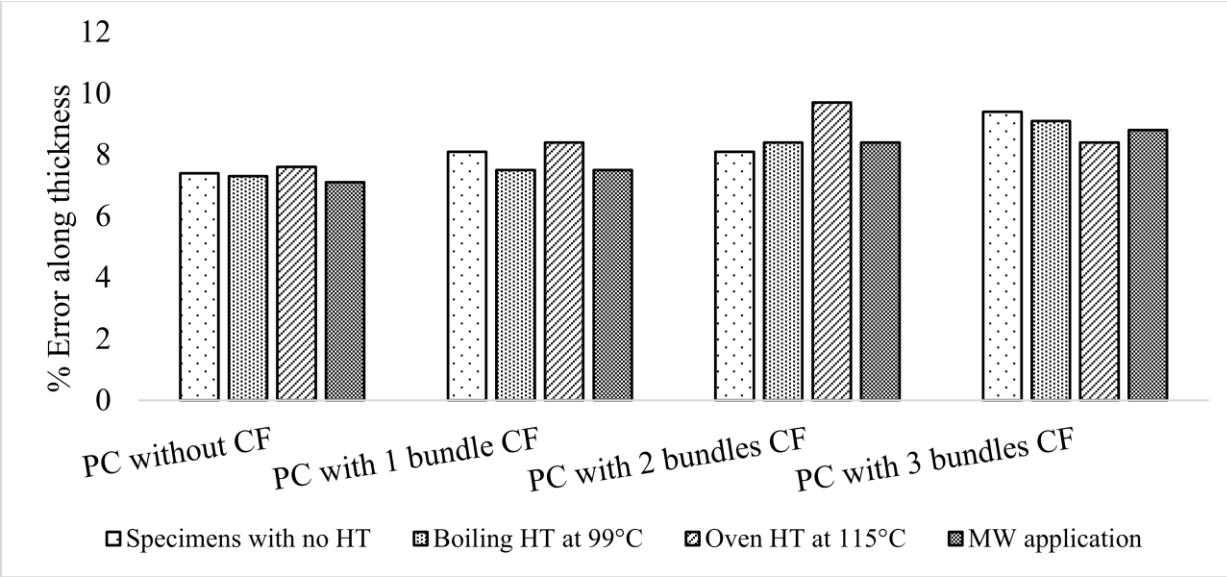

Figure 4. 6 Error percentage of 3D printed PC specimens with and without CF for all specimens under four different post processing heat treatment: along thickness. Note that average inaccuracy increased with increased number of CF bundle.

FDM printed specimens. Those are: position of printed specimen on build sheet, printing orientation, printing pause, thermal expansion and cooling rate of polymer. Theoretically, maximum 14.25 % (3*0.152/3.2*100) of error along thickness are expected for PC with three bundles of CF; 0.152 mm is the thickness of CF. But the filling of the voids (fig SEM) with the melted filament beads reduces the displacement rate of materials and resulted in 9.7% inaccuracy along thickness. It was expected that the increase of CF bundle will affect dimensional inaccuracy because of the absence of cavity and that is visible from the figures also. But no such trend was found accomplish that the increase of CF will necessarily induce more inaccuracy. One possible solution to reduce the inaccuracy is to use cavity of the same thickness of the CF after the calibration of printing layer height.

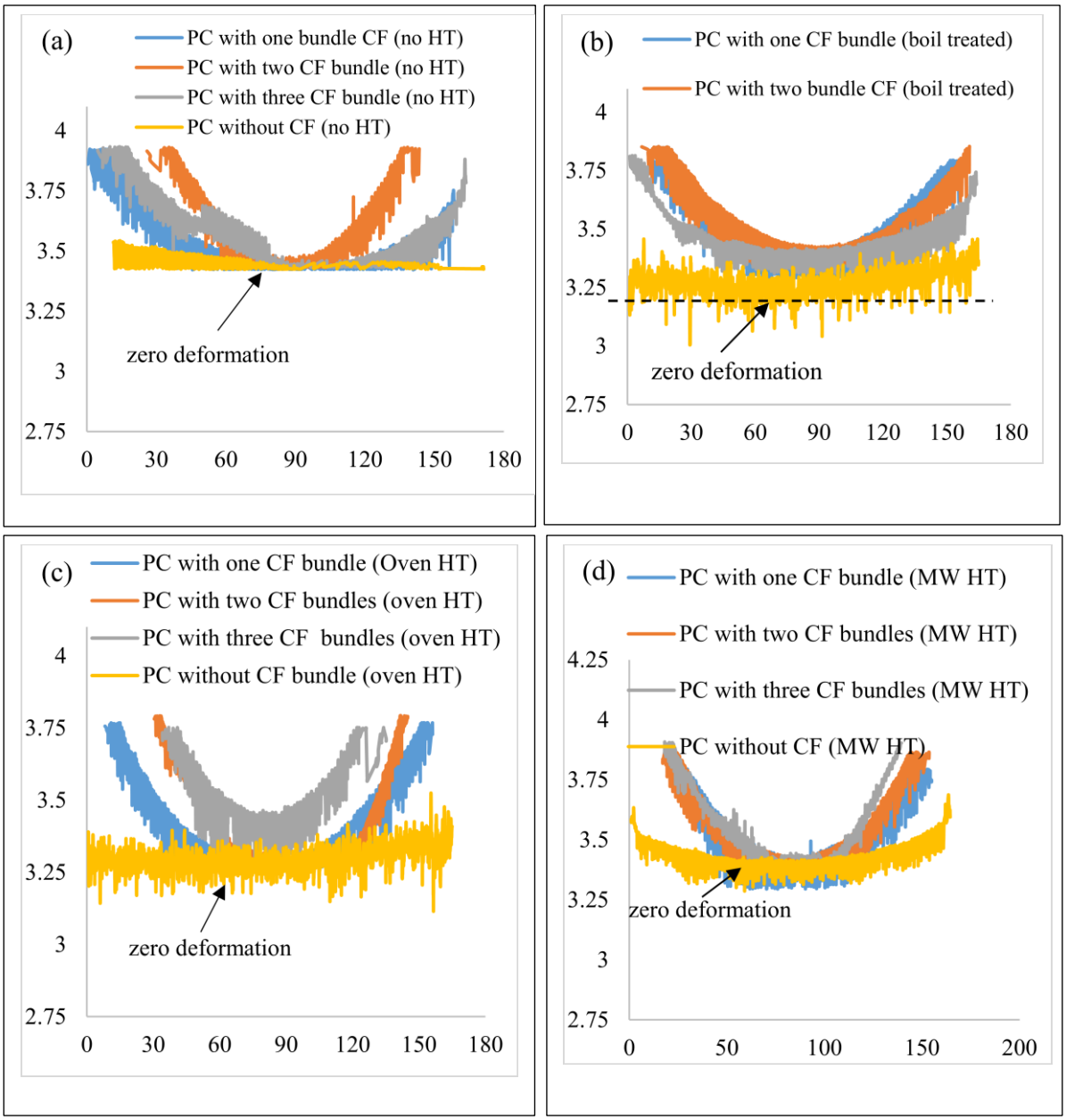

Figure 4. 7 Warp behavior of all samples with an without CF for (a) no HT, (b) water-boiled, (c) oven HT, and (d) MW HT

4.3.2 Warp Test

Figure 4. 7 shows the warpage behavior of different sample sets with three HT post processes and without any HT. Neat PC specimen was visibly lot straighter than PC with CF

bundles. 7a shows a dotted line at 3.37 mm as base line where minimum warpage was found for neat PC and the maximum warpage was noticed for PC with three bundle CF (3.92 mm) which is 0.55 mm more than the base line. That may be explained with the concept of thermal expansion rate. CF has negative thermal expansion rate of -1×10^{-6} mm/mm/°C, but PC has a positive one ($\alpha = 68.4 \times 10^{-6}$ mm/mm/°C). After printing, temperature decreases from 145°C to room temperature (23°C) and if thermal expansion properties behaves linearly, PC should contract 1.3 mm and CF should expand 0.02 mm. Because of the strong bonding between PC-CF and expansion mismatch, PC cannot move linearly with the increasing of length of CF and causes warp behavior. Another thing to observe that PC with one and two CF bundle showed maximum difference of 0.55 mm and 0.51 mm from base line. The warpage created by the inclusion of one CF bundle was similar for PC with two and three CF bundles. The trend illustrates that warpage is affected only by inclusion of first CF bundle in PC and the addition of further CF doesn't affect warpage significantly. Figure 4. 7b shows that water boiled heat treated specimen has lower deformation value from samples without HT when compare to maximum and minimum values. PC without CF showed minimum deformation and PC with one, two, and three bundles CF showed maximum deformation of 0.79 mm, 0.85 mm and 0.81 mm from the base line, respectively. Figure 4.7c explains the warp behavior of oven treated samples. Baseline was set again from neat oven treated PC specimen.

PC specimen at its minimum point and PC with one, two and three CF bundle showed maximum deformation of 0.63 mm, 0.65 mm, 0.61 mm, respectively from that zero deformation line. MW treated specimens with CF bundle showed identical warpage properties from the water boiled and oven heat treated specimens. PC with one, two, and three CF bundles showed maximum

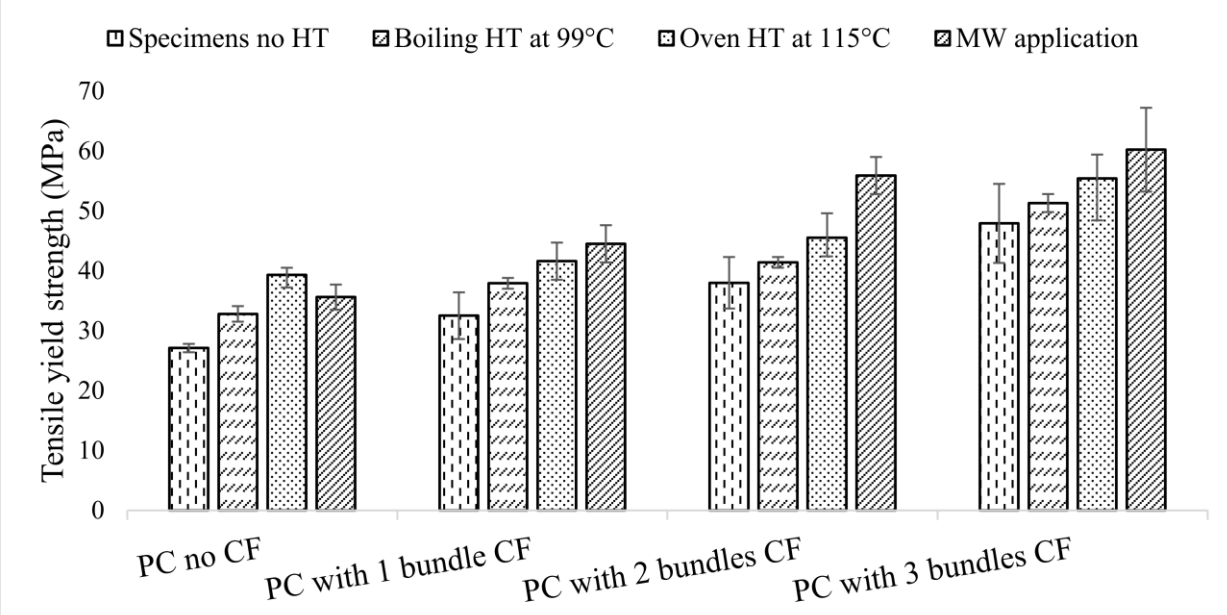

Figure 4. 8 Average results of tensile yield strength of 3D printed specimen for all four sets of samples with under four different heat treatment process with sample standard deviation (±σ) (five specimens used for each set)

deformation of 0.51 mm, 0.51 mm and 0.61 mm when compared to the baseline set from the lowest point of the curve of MW treated neat PC specimen (3.29 mm) (figure 4.7d).

Warpage can be mixed consequence of bending, twisting, internal stress and residual stress. In our study, impact of those factors weren't studied separately but seemingly, these factors were more primitive with the inclusion of first CF. But with two and three CF bundles, such factors can be partially balanced on either side of the CF because of the equal amount of PC material at above and below the specimen.

4.3.3 Tensile Test

Figure 4. 8 shows the average tensile yield strength of all sets of 16 different samples specimens. Note that, the 16 different samples differs with the number of CF present in the PC

specimen and the HT. In each case, PC- CF specimens without HT showed increase of yield strength with the increased number of CF bundles. Note that, a 77% increase in tensile yield strength was found with three CF bundle than the one without any CF among samples without HT.

The heat-treated specimen with CF bundle showed consistency in result. Specimen under boiling application showed better strength when compare to PC- CF specimens with same number of CF bundles and without any HT. Note that, PC with three CF bundles under boiling heat treatment showed 56.4% and 35.4% increase of tensile yield strength respectively than untreated PC without CF and with one CF bundle.

The oven heat treated specimen showed improvement of tensile yield strength with the increase of CF bundle. The strength of oven treated PC with three CF bundle was 55.4 MPa which is 104.4% and 70.5% more respectively than the strength of untreated neat PC and untreated PC with one bundle CF. Note that, oven heat treatment doesn't allow heat to penetrate through the material surface unless it's a slow heating for long term but the porosity present in FDM printed parts allows heat energy to cross the inner surface boundary of specimen. Note that, CF has a negative thermal expansion rate and on the other hand PC has positive expansion rate which means upon application of heat in furnace (an hour at 115°C), CF shrank but the PC specimen expanded allowing better bonding between PC-CF. Oven heat treated PC with three CF bundle showed 69% and 8% increase of strength than boiling treated PC with one and three CF. For boiling, which is mainly an application of forced convection, can import less amount of heat inside. For the entire period of boiling heat treatment, temperature was 99°C at 1 atm pressure and due to continuous movement of forced convection of water, there was no chance for heat or wave energy to penetrate the specimen and this explains the lower strength property of boiling treated specimen compare to the oven treated one.

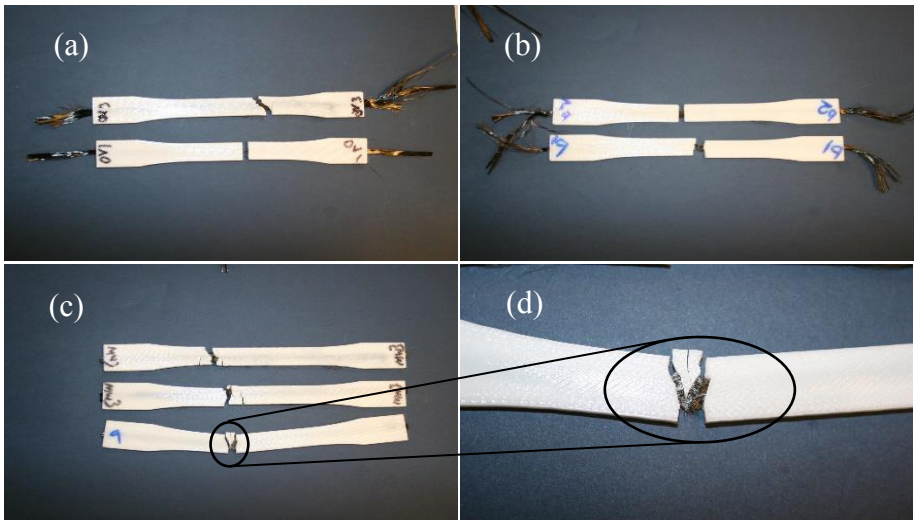

Figure 4. 9 3D printed PC fractured specimen with CF under (a) water boiled, (b) oven, (c & d) microwave heat treatment

Among all set of samples with CF, MW treated specimen showed maximum tensile yield strength. MW treated PC with one, two and three bundles of CF showed 64%, 106% and 122% increase in strength than untreated neat PC (without any CF). The ability of MW energy to penetrate through the specimen ensures maximum heat to reach the lower-mid section of the specimen. The wave energy absorption power and contraction property of CF with increase of heat energy, ensures improved bonding between PC and CF. Figure 4. 9 highlights the fracture surface where boil and oven treated CF reinforced PC specimen shows two separate portions connected by CF after being fractured (a & b). But along with the two divided portion, an extra attached portion is visible (c &d) with CF after being fractured due to tensile test in MW treated specimen which refers to stronger bonding between PC and CF. Thostenson et al. (1999) [44] explained the high strength of carbon fiber reinforced composites under MW treatment. He explained that during MW application in a CF reinforced polymer composite, MW selectively couple with the material with higher dielectric loss (which is CF in this study). As MW tends to couple with the CF, the

Table 4. 2 t-test results of average tensile results of tensile yield strength comparing PC specimens without any heat treatment (HT) and with MW HT

sample 1	sample 2	*t* statistical	*t* critical	*p*-value (two tail)
Neat PC without HT	Neat PC MW HT	17.9	2.8	0.00006
Neat PC without HT	PC with 1 bundle CF MW HT	8.8	2.8	0.0009
Neat PC without HT	PC with 2 bundle CF MW HT	13.3	2.8	0.0002
Neat PC without HT	PC with 3 bundle CF MW HT	13.4	2.8	0.0002
PC with 1 bundle CF without HT	PC with 1 bundle CF MW HT	5.6	2.4	0.001
PC with 1 bundle CF without HT	PC with 2 bundle CF MW HT	9.3	2.6	0.0003
PC with 1 bundle CF without HT	PC with 3 bundle CF MW HT	8.1	2.6	0.0005
PC with 2 bundle CF without HT	PC with 2 bundle CF MW HT	6.5	2.8	0.003
PC with 2 bundle CF without HT	PC with 3 bundle CF MW HT	7.4	2.8	0.002
PC with 3 bundle CF without HT	PC with 3 bundle CF MW HT	3.7	2.8	0.02

fibers heat the nearest interface through conduction and resulted better tensile strength properties because of the strong bonding between CF and polymer.

Table 4. 2 shows that the tensile yield strength of untreated and MW treated specimens of all the samples (i.e., PC with no CF, PC with one, two, and three CF bundles) were significantly different (p-value < 0.05) when compared to one another. Therefore, it rejects the null hypothesis that there is no difference in the tensile yield strength between each group is rejected.

Neat PC sets without CF didn't maintain the same strength trend of PC-CF specimens' for the samples with oven and MW heat treatment. The strength of oven and MW treated specimens were 39.3 MPa and 35.6 MPa, respectively. That proves the introduction of MW in CF-PC

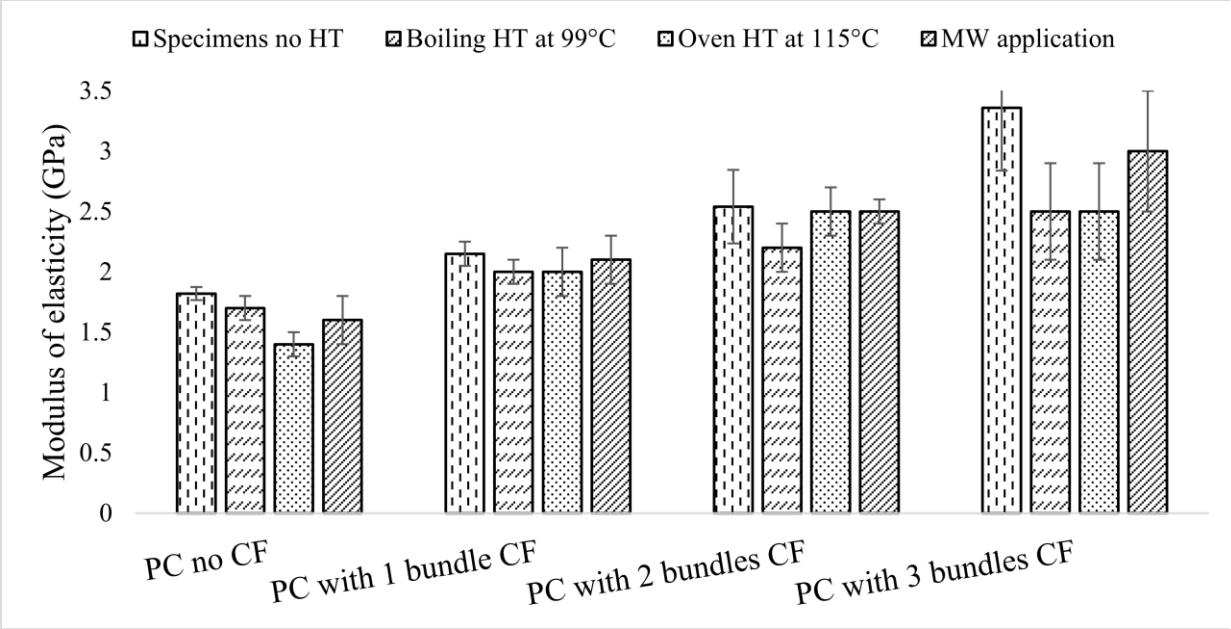

Figure 4. 10 Results of modulus of elasticity of 3D printed specimens with and without CF of all different sets of samples with different post processing heat treatment with sample standard deviation (±σ) (five specimens used for each set)

specimens resulted stronger bonding because of the penetration of MW through the specimen, and high MW energy absorption power of CF and resulted higher strength than the other samples.

The coefficient of variation (CoV= standard deviation/ mean) increased with the number of CF bundle and was maximum for untreated PC with three bundles of CF (0.14). Note that, for each set of samples, maximum CoV was observed for the untreated PC-CF specimen. The heat absorbing property of CF under HT ensured better bonding with PC and this phenomenon improves bonding of water boiled, oven and MW treated specimens. For untreated system, manually applied non-uniform heat resulted inconsistent bonding between PC, and CF and increased standard deviation.

Table 4. 3 Results for specific strength of 3D printed samples under four different post processing heat treatment

Sets	Heat Treatment (HT)	Tensile Yield Strength (MPa)	Mass	Specific Strength, SS (MPa/g)
PC with no CF	No HT	27.1	9.4	2.9
	Boiling HT	32.8		3.5
	Oven HT	39.3		4.2
	MW HT	35.6		3.8
PC with one bundle CF	No HT	32.5	9.5	3.42
	Boiling HT	37.9		4
	Oven HT	41.6		4.4
	MW HT	44.5		4.7
PC with two bundle CF	No HT	38	9.6	4
	Boiling HT	41.4		4.3
	Oven HT	45.5		4.7
	MW HT	55.9		5.8
PC with three bundle CF	No HT	47.9	9.7	4.9
	Boiling HT	51.3		5.3
	Oven HT	55.4		5.7
	MW HT	60.2		6.2

The tensile yield strength of MW treated PC with one bundle CF is 44.5 MPa which is almost equals the strength of untreated PC with three bundle CF specimen (47.9 MPa). The strength of oven treated and MW treated PC with two bundle CF were 45.5 MPa and 55.9 MPa which is comparable with the strength of untreated PC with three bundle CF. So, proper heat treatment of specimen can eliminate the urge to embed multiple CFs for better strength.

The yield strength of injection molded PC specimen is 58-63 MPa. MW treated PC with three bundle CF showed the strength of 60.2 MPa. This eliminates one of the major drawback of

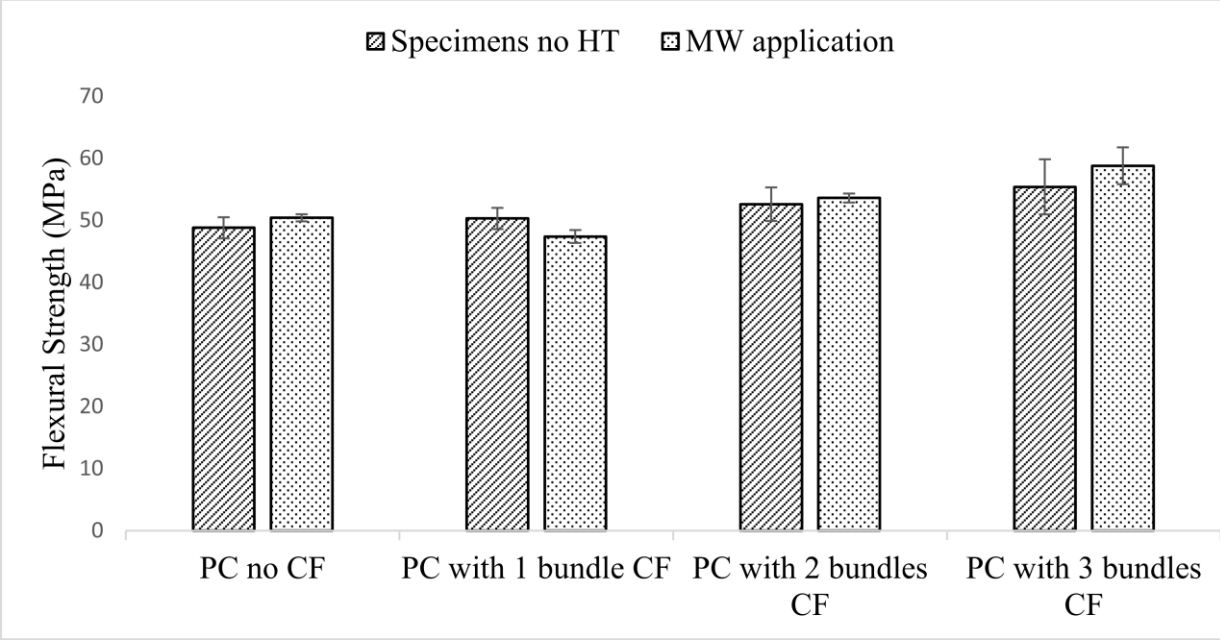

Figure 4. 11 Results of flexural stress of 3D printed specimens with and without CF under MW HT and no HT with sample standard deviation (±σ) (five specimens used for each set)

3D printing technology because MW treated 3D printed specimen ensures both strong and complex shaped 3D printed part.

Figure 4. 10 shows that increased bundle of CF results in increased modulus of elasticity. For each set, PC with CF bundle without any treatment showed maximum elasticity. Strain rate at yield point varied from 1% to 3% and at fracture point varied from 4% to 6%.

Table 4. 3 shows 114% increase of specific strength (SS) of MW treated PC with three bundle CF (6.2 MPa/g) than the neat PC without CF (2.9 MPa/g). SS increased with increased number of CF bundle and MW treated PC- CF specimen showed higher SS than the other samples (no treatment, boil, and oven) from the same set.

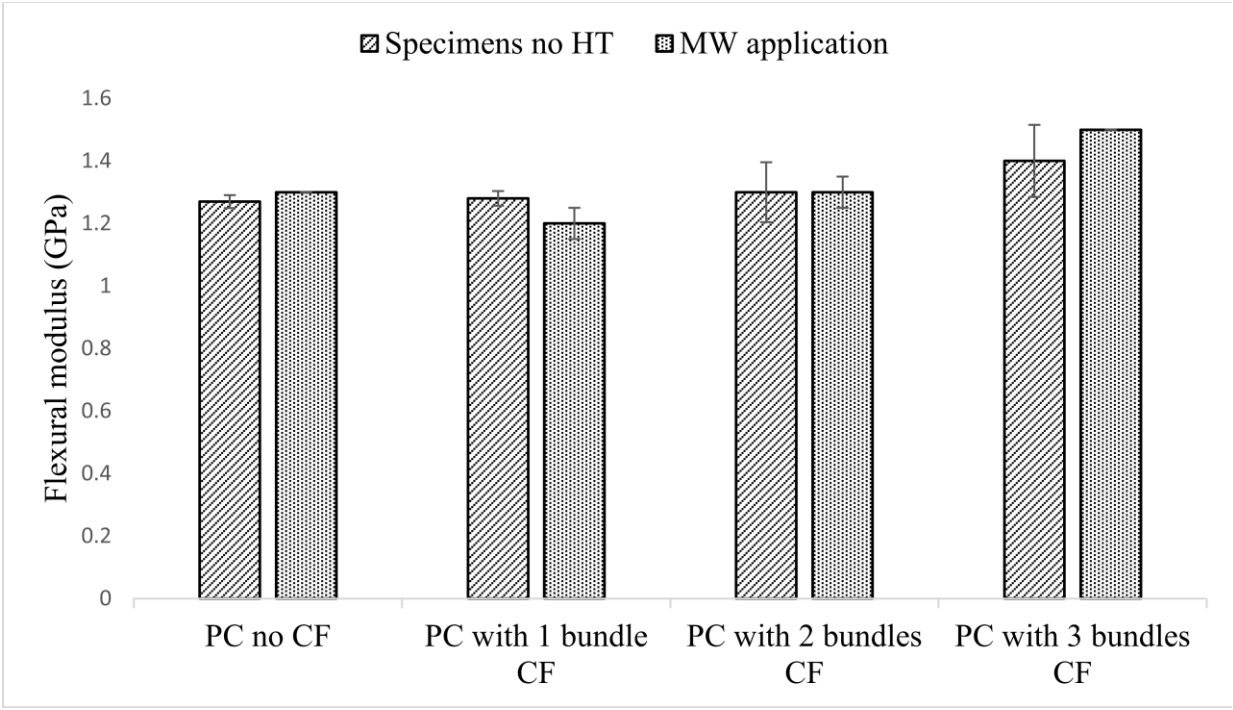

Figure 4. 12 Results of flexural modulus of 3D printed specimens with and without CF under MW HT and no HT with sample standard deviation (±σ) (five specimens used for each set)

4.3.4 Flexural test

Figure 4. 11 shows the result of flexure test of PC with one bundle, two bundles, and three bundles of CF. Note that, only MW HT was done to compare with the samples without any HT. MW heat treated PC with three bundles of CF/ M_3 (58.8 MPa) showed an increase of 17% flexural strength than neat PC without any HT/ N_0 (48.8 MPa). Note that, at the three-point bending test, none of the specimens fractured and the stress was noted from the 5% flexural strain (figure 4. 4b). PC with one bundle CF and neat PC without CF bundle showed almost same flexural stress properties but PC with two bundle and three bundles of CF showed improved strength property pointing out the fact that the impact of CF is significant when it is close to the boundary of the part. Effect of MW HT was not significant for all the samples and maximum 6.1% improvement

was observed for M_3 compare to N_3. Figure 4. 12 shows that maximum flexural modulus was for M_3 (1.5 GPa) which is 15.4% higher than N_0 (1.3 GPa). One important observation is the standard deviation for both flexural strength and modulus of MW heat treated parts were lower than the untreated samples.

4.3.5 Porosity and bonding

Figure 4. shows the state of porosity specimens for all 16 different sets of samples where the first, second, third and fourth rows represent no HT, boiling HT, oven HT, and MW heat treated specimens, respectively. For each row, increase of CF showed regions without porosity which here is named as 'Zero Pore Regions' (ZPR). PC with no CF showed inconsistent pores and PC with three bundle CF showed least number of voids for three HT conditions and even without HT when comparing at a same heat treatment condition. The reason behind is the disturbance caused by the CF in the printing process for embedding CF due to the absence of cavity. CF has a thickness of 0.154 mm which is more than half of one layer (0.254) of printing in FDM 400mc. With the inclusion of first CF, the next layer printing faces insufficient spaces and in the process fills out the voids with the applied pressure from the printing tip. Embedding of two and three CF bundles occupy 0.308 mm and 0.462 mm which covers more than one layer of printing and these 813 mm^3 and 1220 mm^3 [0.462*(13+19)/2*165] materials fills the voids because of the insufficient space and applied pressure from the printing tip.

Figure 4. shows boil treated PC with one bundle of CF, small region above the CF has no voids (fig f) but for oven and MW treated PC with one bundle CF, percentage of porosity was higher. Note that, PC with MW treated one bundle CF had the higher tensile yield strength than oven treated specimen where boiling heat-treated specimen showed minimum strength. This refers to the better bonding of PC- CF in MW and oven treated specimens because of the higher heat

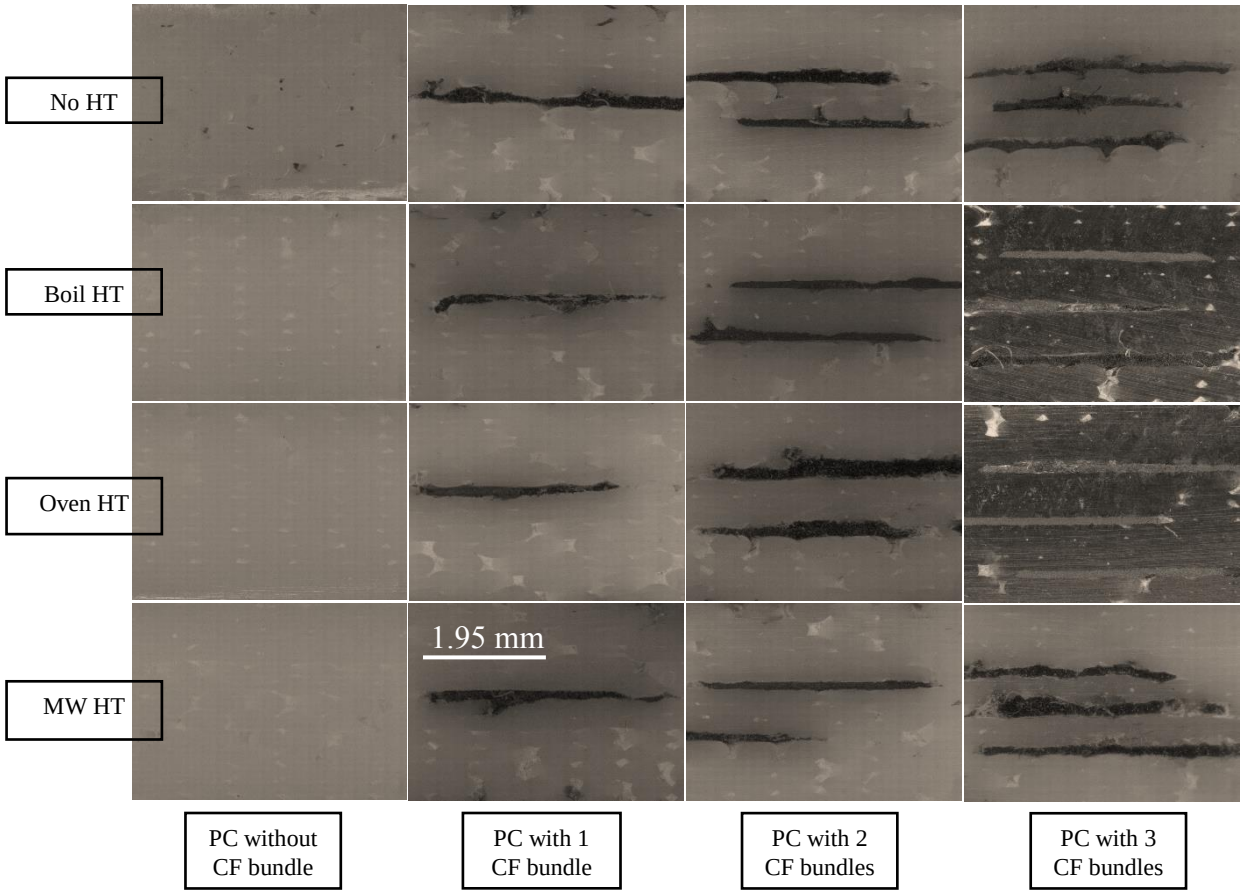

Figure 4. 13 Micrograph of all 16 different sets of samples at mid portion. Note that, all the rows have same treatment mentioned at the starting of row and all the column represents the same number of CF. Note that, the scale is same for all the figures.

energy absorption capacity of CF. But for PC with two and three CF bundles (4^{th} row), oven and MW treated specimens showed less amount of porosity than boil heat treated specimen.

Figure 4. 14 shows the porosity state of all samples at corners of the specimen. This section is important to monitor the impact of embedded CFs through the whole layer and in next few layers. The corner portion, considering all HTs, PC with three bundle CF showed minimum amount of porosity than PC with one and two CF bundles. The calculation showed in the first

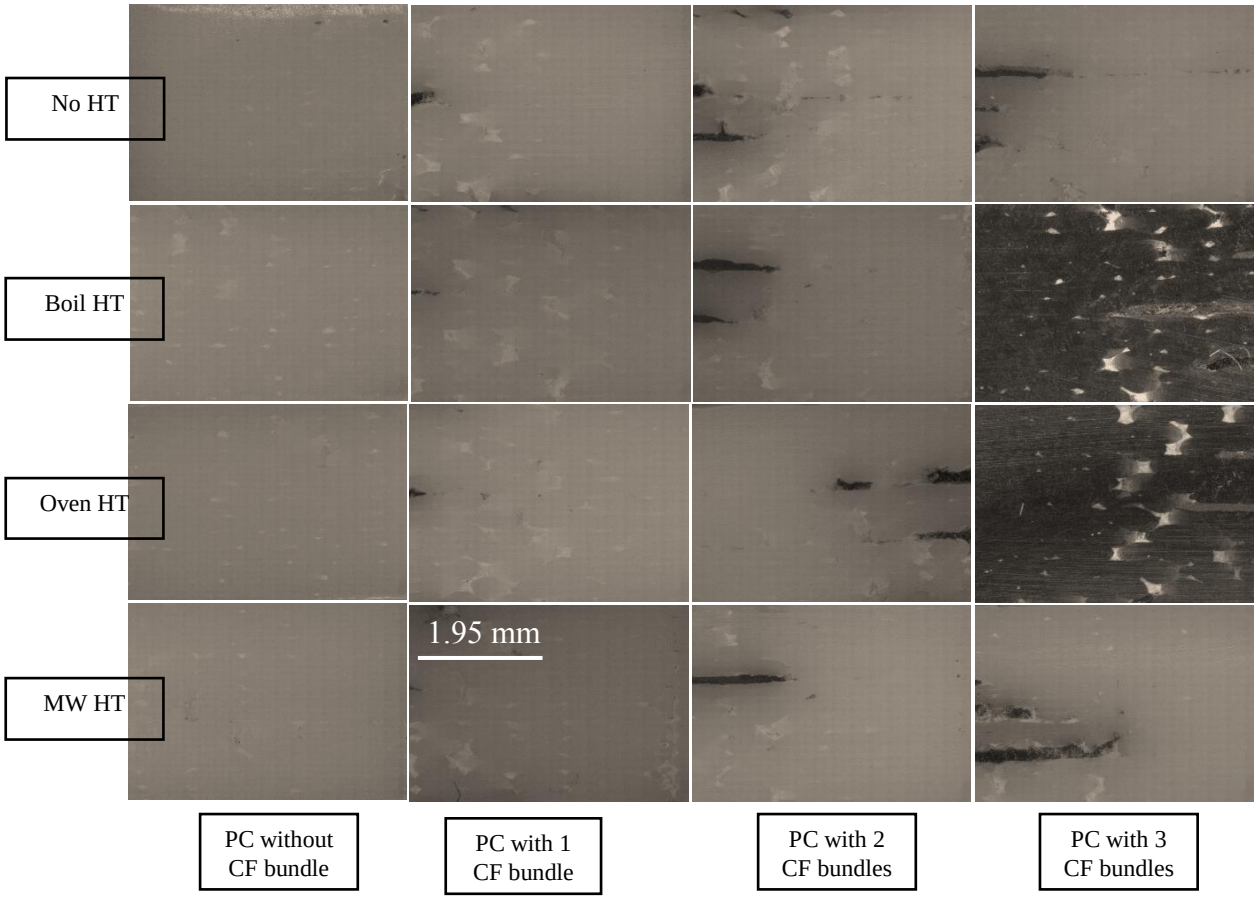

Figure 4. 14 Micrograph of all 16 different sets of samples at side portion near boundary. Note that, all the rows have same treatment mentioned at the starting of row and all the column represents the same number of CF. Note that, the scale is same for all the figures.

paragraph of this section clearly demonstrate this phenomenon. The last row of the Figure shows that pore size was smaller for MW treated PC specimen with CF bundles when compare to oven and boiling heat-treated specimens. That ensures better neck growth of MW treated specimens.

4.4 Conclusion

To the author's knowledge, this is the first publication wherein heat treatment post processing of continuous CF reinforced 3D printed PC composite. Sixteen different sets of

samples, depending on number of CF and HT, were fabricated and MW treated PC with three bundles CF showed 122%, 20.5% and 114% increase of tensile yield strength, flexural strength and specific strength, respectively, compare to neat PC specimen without any HT. MW treated PC with three bundles CF showed equal tensile yield strength (60.2 MPa) with injection molded PC (58-63 MPa) specimen. The mismatch of thermal expansion between PC and CF during cooling to room temperature resulted warpage but it did not necessarily increased with the addition of further CF.

Acknowledgements

The fabrication, characterization and heat treatment presented here was conducted at The University of Texas at El Paso (UTEP) within the W.M. Keck Center for 3D Innovation (Keck Center). The authors acknowledge the contribution of Lluvia Herrera for her assistance and support during experimentation.

References

[1] S. Kalia, B. Kaith and I. Kaur, "Pretreatments of natural fibers and their application as reinforcing material in polymer composites—a review," *Polymer Engineering & Science*, vol. 49, *(7)*, pp. 1253-1272, 2009.

[2] H. L. Tekinalp *et al*, "Highly oriented carbon fiber–polymer composites via additive manufacturing," *Composites Sci. Technol.*, vol. 105, pp. 144-150, 2014.

[3] F. Ning *et al*, "Additive manufacturing of carbon fiber reinforced thermoplastic composites using fused deposition modeling," *Composites Part B: Engineering*, vol. 80, pp. 369-378, 2015.

[4] W. Zhong *et al*, "Short fiber reinforced composites for fused deposition modeling," *Materials Science and Engineering: A*, vol. 301, *(2)*, pp. 125-130, 2001.

[5] X. Tian *et al*, "Interface and performance of 3D printed continuous carbon fiber reinforced PLA composites," *Composites Part A: Applied Science and Manufacturing*, vol. 88, pp. 198-205, 2016.

[6] C. Yang *et al*, "3D printing for continuous fiber reinforced thermoplastic composites: mechanism and performance," *Rapid Prototyping Journal*, vol. 23, *(1)*, pp. 209-215, 2017.

[7] G. W. Melenka *et al*, "Evaluation and prediction of the tensile properties of continuous fiber-reinforced 3D printed structures," *Composite Structures*, vol. 153, pp. 866-875, 2016.

[8] K. Mori, T. Maeno and Y. Nakagawa, "Dieless forming of carbon fibre reinforced plastic parts using 3D printer," *Procedia Engineering*, vol. 81, pp. 1595-1600, 2014.

[9] Torres, J., Cotelo, J., Karl, J. and Gordon, A.P., 2015. Mechanical property optimization of FDM PLA in shear with multiple objectives. Jom, 67(5), pp.1183-1193.

[10] Salmoria, G.V., Ahrens, C.H., Beal, V.E., Pires, A.T.N. and Soldi, V., 2009. Evaluation of post-curing and laser manufacturing parameters on the properties of SOMOS 7110 photosensitive resin used in stereolithography. Materials & Design, 30(3), pp.758-763.

[11] D. Espalin Jr, *Development of a Multi-Material, Multi-Technology FDM System for Process Improvement Experimentation.* 2012.

[12] E. Thostenson and T. Chou, "Microwave processing: fundamentals and applications," *Composites Part A: Applied Science and Manufacturing,* vol. 30, *(9),* pp. 1055-1071, 1999.

[13] H. S. Lee *et al,* "Design of microwave plasma and enhanced mechanical properties of thermoplastic composites reinforced with microwave plasma-treated carbon fiber fabric," *Composites Part B: Engineering,* vol. 60, pp. 621-626, 2014.

[14] Y. Liu *et al,* "Preparation and properties of cobalt oxides coated carbon fibers as microwave-absorbing materials," *Appl. Surf. Sci.,* vol. 257, *(17),* pp. 7678-7683, 2011.

[15] R. Anitha, S. Arunachalam and P. Radhakrishnan, "Critical parameters influencing the quality of prototypes in fused deposition modelling," *J. Mater. Process. Technol.,* vol. 118, *(1-3),* pp. 385-388, 2001.

[16] C. Ziemian and P. Crawn III, "Computer aided decision support for fused deposition modeling," *Rapid Prototyping Journal,* vol. 7, *(3),* pp. 138-147, 2001.

[17] A. Armillotta, M. Bellotti and M. Cavallaro, "Warpage of FDM parts: Experimental tests and analytic model," *Robot. Comput. Integrated Manuf.,* vol. 50, pp. 140-152, 2018.

[18] A. Gregorian *et al,* "Accuracy improvement in rapid prototyping machine (FDM-1650)," in *Solid Freeform Fabrication Proceedings,* 2001, .

[19] S. J. Kalita *et al,* "Development of controlled porosity polymer-ceramic composite scaffolds via fused deposition modeling," *Materials Science and Engineering: C,* vol. 23, *(5),* pp. 611-620, 2003.

[20] ASTM Committee F42 on Additive Manufacturing Technologies and ASTM Committee F42 on Additive Manufacturing Technologies. Subcommittee F42. 91 on Terminology, *Standard Terminology for Additive Manufacturing Technologies.* 2012.

[21] D. ASTM, "638-03: Standard Test Method for Tensile Properties of Plastics," *Current Edition Approved Apr,* vol. 1, pp. 1-16, 2008.

[22] ASTM, D., 2008. 618. Standard practice for conditioning plastics for testing. ASTM Standard. ASTM International: West Conshohocken PA.

[23] R. Pennington, N. Hoekstra and J. Newcomer, "Significant factors in the dimensional accuracy of fused deposition modelling," *Proc. Inst. Mech. Eng. Part E J. Process Mech. Eng.,* vol. 219, *(1),* pp. 89-92, 2005.

Appendix A: Permission to Include Journal Paper from the Additive Manufacturing Journal

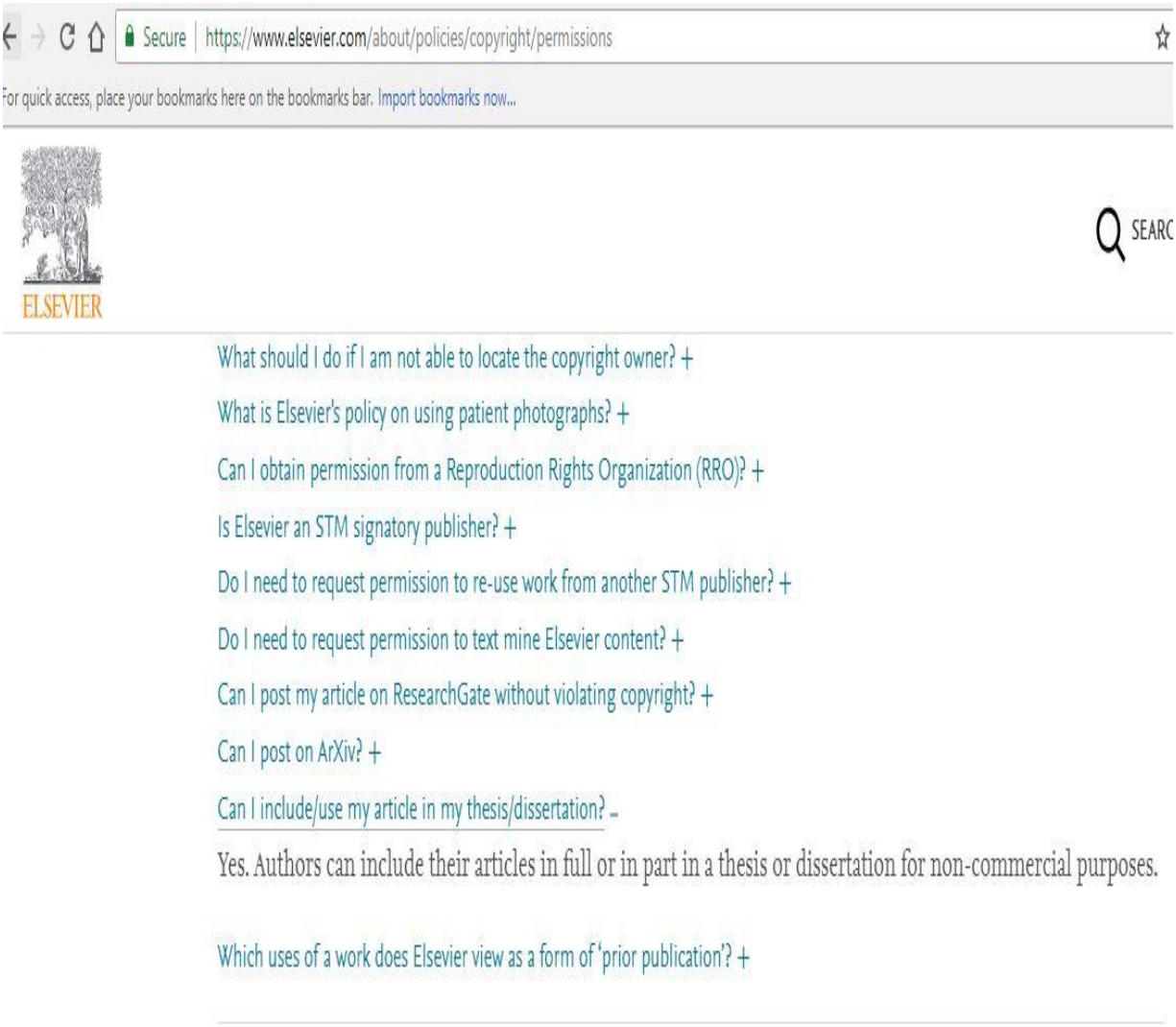

Vita

Md Naim Jahangir was born on November 24, 1992 in a small village of Bogra in Bangladesh. He is the youngest son of Mrs. Firoza Khatun and Mohammad Ali Mondal (1952-2010). Naim obtained his secondary and higher secondary degrees from Ideal School and College, Motijheel, Dhaka and Notre Dame College, Dhaka with talent pool scholarships. He obtained a Bachelor of Science degree in Mechanical Engineering from Bangladesh University of Engineering and Technology (BUET) in September 2015. During his graduation study in University of Texas at El Paso (UTEP), Naim was active in both research work and study. He worked as a Teaching Assistant for several classes and then was employed as a Research Assistant in W. M. Keck Center. He has already submitted a journal paper in Journal of Additive Manufacturing and another one is in the pipeline for submission. He took part and presented his work in UTEP Grad Expo 2017 and Southwest Emerging Technology Symposium (SETS) 2018. He designed and fabricated a foil application tool for a low cost muslti 3D system, a project of National Center for Defense Manufacturing and Machining (NCDMM).

Email: mnjahangir@miners.utep.edu

This thesis was typed by Md Naim Jahangir.